Theses, Dissertations and Capstones

2007

Atmospheric smog modeling, using EOS Satellite ASTER Image Sensor, with feature extraction for pattern recognition techniques and its correlation with In-situ ground sensor data

Parthasarathi Roy

Atmospheric Smog Modeling, Using EOS Satellite ASTER Image Sensor, with Feature Extraction for Pattern Recognition Techniques and Its Correlation with In-*situ* Ground Sensor *Data*

Thesis submitted
by
Parthasarathi Roy

In partial fulfillment of the requirements for the degree of

Master of Science

**In
Physical Science**

**With Emphasis in
Geobiophysical Modeling and Remote Sensing**

Submitted on the 9th day of May, 2007

To the Faculty of the Graduate College of

Marshall University, Huntington, West Virginia

Abstract

Atmospheric pollution was previously considered as a 'Brown Cloud' phenomenon restricted to industrialized urban regions. Studies in field stations and satellite observations made since the last decade revealed that it now spans continents and ocean basins world wide. The objective of this research investigation is to assess atmospheric pollutants in the troposphere and their spectral characteristic signatures by using high-spectral and spatial resolution Earth Observation System (EOS) satellite imaging sensor Advanced Spaceborne Thermal Emission and Reflection Radiometer (ASTER) data and to find correlations with ground sensor observations. Ground sensor data are imported into a geodatabase for spatial reference. Raw ASTER data are georegistered and geocorrected by image-to-image registration with a known geo-corrected image. Data Fusion, Principal Component Analysis (PCA), Density Slicing, Band Ratioing, and Band-pass Filtering techniques are applied to extract features in the ASTER datasets. Spectral signatures in graphical form of the atmospheric features are obtained in ER-Mapper 7.1 geospatial software (ER-Mapper, 2006) and compared both in short wave infra-red (SWIR) and thermal infra-red (TIR) bands. It is observed that the impact of air pollutants from polluting sources are not just confined to the areas under investigation but extend further as pollutants are transported by wind to greater distances. Correlation between ground sensor pollution level and ASTER image pollutants pixel digital numbers are obtained by creating a general linear model in the PROC-GLM program in Statistical Analysis System (SAS) user software. Despite broader bandwidth of ASTER as compared to hyperspectral satellite systems, an excellent high correlation is observed in spectral response of all TIR bands and moderate correlation with SWIR bands of ASTER

with ground sensor monitoring in all the three areas, i.e. San Francisco Bay area and Los Angeles, in California, and in Charleston in West Virginia. Future investigation is envisioned to study the subtle differences in spectral signatures of air pollutants by using hyperspectral satellite data and nanotechnology based sensors.

Acknowledgements

consistent and interactive support. Finally I am grateful to my parents, my lovely beloved wife Munmun and all other family members whose good wishes have enabled me to persevere through my two wonderful years in Marshall University.

Table of Contents

List of Figures

List of Tables

List of Abbreviations

ALA: American Lung Association

AOT: Aerosol Optical Thickness

ASTER: Advanced Spaceborne Thermal Emission and Reflection Radiometer

AVHRR: Advanced Very High Resolution Radiometer

BAMS: Beta Attenuation Method Sampler

CCD: Charged Couple Detectors

CH_4:   Methane

CNT: Carbon Nano Tubes

CO: Carbon Monoxide

DN: Digital Numbers

DOQQ: Digital Orthophoto Quarter-Quadrangles

EOS: Earth Observing System

EPA: Environmental Protection Agency

ETM+:   Enhanced Thematic Mapper Plus

GHG: Green House Gases

HDF: Hierarchical Data Format

HgCdTe: Mercury-Cadmium-Telluride

HITRAN: High-resolution Transmission Molecular Absorption

HNO3:   Nitric Acid

HNO2:   Nitrous Acid

JPL: Jet Propulsion Laboratory

L1A:	Level 1 A
METI:	Ministry of Economy, Trade and Industry
MODIS:	Moderate Resolution Imaging Spectrometer
MSS:	Multi-Spectral Scanner
NASA:	National Aeronautics and Space Administration
NCDC:	National Climatic Data Center
NOAA:	National Oceanic and Atmospheric Administration
NO_x:	Oxides of Nitrogen
PAN:	Proxy Acyle Nitrates
PCA:	Principal Component Analysis
PM:	Particulate Matter
PtSi-Si:	Platinum Silicide-Silicon
RGB:	Red green and blue
$SO_{2:}$	Sulphur Dioxide
SPC:	Science Policy Council
SWIR:	Short Wave Infra Red
TEOM:	Tapered Element Oscillating Microbalance
TIR:	Thermal Infra Red
TM:	Thematic Mapper
UNEP:	United Nations Environmental Program
USGS:	United States Geological Survey
UTM:	Universal Transverse Mercator
VNIR:	Visible and Near Infra-Red
WHO:	World Health Organization
μ m:	Micro-meter

Chapter 1

Introduction to Atmospheric Smog Modeling

1.1. Air Pollutants

Atmospheric pollution was previously considered as a 'Brown Cloud' phenomenon restricted to industrialized urban regions. Studies in field stations and satellite observations made since the last decade revealed that brown cloud (haze or smog) phenomenon which is normally associated with urban regions now spans continents and ocean basins worldwide (Ramanathan and Ramanna, 2003). Smog has potentially large impact on both radiative heating and the regional gas phase chemistry of the region. (Lelieveld, J. et al., 2001). Anthropogenic activities are considered to be as the primary cause of pollution in the atmosphere. Gaseous air pollutants, like NO_x, SO_2, CO, and CH_4, are some of the primary air pollutants in urban and industrial areas. Secondary pollutants are created from the primary pollutants by complex photochemical reactions in the presence of ultra-violate (UV) radiation forming free radicals in the atmosphere (UNEP- United Nations Environmental Program, 2005). Sulfur and oxides of nitrogen (NO_x) from industrial emissions transforms into ammonium sulfate and nitrate. In the presence of atmospheric moisture, NO_x transforms into HNO_3 and HNO_2 (WHO, 2000). Air pollutants can be found in all three physical phases: solid, liquid or gaseous. When pollutants are in fine solid state floated in the atmosphere, they are called aerosols or particulates, which depending on their diameter, can be non-respirable particles (of dimension greater than $10\,\mu$m), respirable particulate matter (PM_10 of dimension less than $10\,\mu$m), or inhalable particulate matter (PM_2.5 of dimension less than 2.5 μm).

PM_10 and PM_2.5 can remain in suspension in the air for hours or days and can be transported by the wind to significant distances. Both particulate matters (PM) categories have been shown to cause health effects but the latter (i.e. PM_2.5) are the most damaging because they can penetrate into much deeper parts of the respiratory tract, namely the alveolar regions of the lungs (WHO, 2000). Epidemiological studies have shown a strong and consistent correlation between adverse health effects and air pollution (Pope, 2000). Generally, the atmospheric aerosol is a complex mixture of chemical species consisting of organic and elemental carbon, mineral dust, sulfates, nitrates, dust and fly ash particles, natural aerosols such as sea salt and water (Satheesh and Ramanathan (2001). In North-America and Europe urban fine aerosols typically contain 28% sulfates, 31% organics, 9% BC, 8% ammonium, 6% nitrate and 18% other material with mean mass 32μ g/m^3) (UNEP Assessment Report, 2004). Aerosols are emitted by anthropogenic sources, biogenic sources, and significant industrial emissions. Burning of both fossil fuel and biomass contributes significantly to aerosols or PM concentrations that form smog in the atmosphere (Ramanathan and Ramanna, 2003). In-situ measurements of aerosol chemistry from aircraft and surface stations found that anthropogenic sources (e.g. Biomass burning, fossil-fuel combustion) contribute as much as 75% to the observed aerosol concentration (Ramanathan et al., INDOEX, 2001 and Lelieveld et al. 2000). Observatory and satellite data revealed that organic carbon, carbon black and fly ash contribute more to haze in Asia than SO$_2$ (Lee et al. 2004). The biomass burning creates aerosols, which seldom deposited dry, are instead activated in cloud and cloud nucleating properties. These aerosols control cloud albedo. Scattering albedo increases, as pollution increases, with backscatter fraction decreasing. There is observational evidence that these aerosols can alter cloud properties (Lee et al. 2004).

2

Aerosol radiative forcing depends on hygroscopicity, which in turn depends on aerosol photo-chemistry. Condensation of secondary organic aerosols on nucleation can reduce the hygroscopic properties of particles causing the slow conversion of cloud droplets into precipitation, allowing the convective energy to accumulate and eventually trigger violent storms. Similarly, reducing aerosol pollution, or reversing the effect of the small pollution aerosols by introducing large hygroscopic elemental aerosols can accelerate the early onset of rain (Petaja et al. 2005). Smog is particularly a severe problem in big cities in tropical regions. SO_2 and other Green House Gases (GHGs) contribute to a lesser extent to the formation of smog than aerosols. The entire South Asia SO_2 emission is only 25% of the total United States (US) SO_2 emission, but in South Asia haze is prevalent even in small cities, due to relatively longer dry seasons (Ramanathan and Ramanna, 2003).

1.2 Radiative Forcing

Smog affects the earth's energy budget directly by scattering and absorbing radiation and indirectly by acting as cloud condensation nuclei and, thereby, affecting cloud properties (Yu et al. 2005). The appearance of a pollution layer with more absorption and scattering of solar radiations, particularly long-wave infrared radiations, decreases the atmospheric transmission factor, and changes the radiation fluxes, not only at the ground surface, but also at the top of the atmosphere, thereby significantly perturbing the atmospheric absorption of solar radiation (Ramanathan & Ramanna, 2003). These aerosol-induced changes in the radiation budget are referred to as 'radiative forcing' Furthermore, the pollution layer in atmosphere absorbs as well as emits radiance thus causing a change of the upwelling

radiation. A relatively small proportion of aerosols can play a dominant role not only from reduction in surface solar radiation but also from latent heat fluxes, atmospheric stability and the strength of convection currents (Menon et al 2002). Although uncertainties remain regarding the magnitude of the radiative forcing impact, it is believed that the single scattering albedo of aerosols is sufficiently high to lead to a net cooling, the antithesis of global warming (Lee et al. 2004). But climate models for the past 10,000 years and measurements made in GHGs in glacial and polar ice current, suggests a trend in global warming, the antithesis of hypothesis of Lee (OSU-Climate Group, 2003). Aerosol climate forcing is one of the hardest problems for climate modelers due to unavailability of forcing details (Chung and Ramanathan, 2003).

1.3 Spectral Signature of Common Atmospheric Pollutants:

Spectral signatures of molecules have become major sources of knowledge of the earth's atmosphere. IR absorption spectroscopy has played an important role in the identification of trace pollutants in both ambient air and synthetic smog systems. In absorption spectroscopy, solar radiation transfers its energy to molecules. Molecular vibration and rotation occur when the frequency of rotation and vibration are equal to frequency of solar radiation directed to the molecules. Molecular vibration and rotation causes molecule to absorb the radiation energy.

In this research spectral signatures of common atmospheric pollutants are collected from Jet Propulsion Laboratory (JPL)'s ASTER (Advanced Spaceborne Thermal Emission and Reflection Radiometer) spectral Library, HITRAN (High-resolution Transmission

Molecular Absorption) Database, and USGS (United States Geological Survey) spectral library. Some of the common air pollutants spectral absorption frequencies along with associated ASTER bands are shown in table1.

Table1: Spectral Signatures (absorption frequencies of common air pollutant, and corresponding ASTER bands (JPL, USGS, HITRAN, Herzberg, 1950).

Air Pollutants	Absorption Frequency in μm	ASTER corresponding Band
Carbon Monoxide	2.30-2.34	7,8,9
HNO3	11	14
CH3OH	8.1	10
Hydroxyl Radical	2.1, 2.3-2.34	5,7,9
Zn,Fe-Sulfide	2.3	7
Arsenite	2.1-2.5	5,6,7,8,9
Formaldehyde	5.3	-
SO2	8.1	9,10,11
Cirrus Cloud	2.1	5
Atm. Water Vapor	1.67	4
CaCO3	5.3-12.0	10,11,12,13,14
Particulate Matters	6.0 - 13.0	10,11,12,13,14
Methane	4.6	-

1.4 Satellite Remote Sensing

The Satellite Remote Sensing era started with the launch of Landsat MSS-I (Multi-Spectral Scanner) in 1972 and subsequent Landsat MSS series and Landsat Thematic Mapper (TM) series of satellite revolutionized earth observation from space. Satellite image data has traditionally been unexploited for atmospheric pollution studies. Only in recent years has satellite observation of atmospheric parameters become a prime concern due to increased risk of global climate change (Ramanathan and Ramanna, 2003). Satellite image data consists of earth radiances observed by its sensors in different bands. For thermal infra-red (TIR) bands

the radiances represent a function of the temperature, emissivity of the ground surface and the atmospheric column above and it's surrounding (ASTER Manual, NASA, 2000). Satellite image data can aid in detection, tracking and understanding of pollutant sources and transport by providing observations over large spatial domains, with three dimensional models (3-D Models). It is now possible to acquire, display, and assimilate these valuable sources of data into the air quality assessment process (Belsma, 2004). Satellite data can be used quantitatively to validate air quality models. The pollution assessment of optical atmospheric effects can be quantified in terms of aerosol optical thickness (AOT) of particles with diameter between 0.1 and 2.5 μ m, which can be carried out with an optimal resolution of 500m x 500m over cloud-free part of any satellite images (USGS-Landsat, 1998). With the launch of NASA's Terra satellite system, a part of Earth Observing System (EOS), in December 1999, satellite observation of atmospheric parameters are easier to acquire.

1.5 Previous investigations of Atmospheric Smog modeling

In most of the previous investigations of Atmospheric Smog modeling, satellite images are used to extract air pollution by calculating optical thickness in, either visible spectral ranges or low spectral resolution short-wave infra red (SWIR) and thermal infra red (TIR) ranges (Retalis, 1999) and (Schafer et. al , 2002). Ramanathan and Ramanna (2003) tried to model aerosols in tropical regions of Asia, by low spatial resolution and high spectral resolution, NASA's Moderate Resolution Imaging Spectro-radiometer (MODIS) instrument. Their main concern was the impact of aerosols in regional radiative forcing, and precipitation. Sifakis and Soulakellis (2001) tried to find optical thickness in VNIR and near-IR bands, in

order to monitor haze with low spatial and spectral resolution MODIS data by the 'blurring effect due to scattering and backscattering induced by the aerosols. Ung et al. (2003) tried to investigate the strength of linear relationship between satellite-made observations and air quality parameters using Landsat low spatial and spectral resolution with very few channels. They did not use any image processing software to process images. Ahmad and Hashim (2000) tried to correlate with low resolution NOAA 14 AVHRR (Advanced Very High Resolution Radiometer) data in VNIR bands using regression model.

1.6 Objective of the Research Investigation

For satellite systems with high spatial and spectral resolution and sophisticated hardware and software, it is now possible to accurately measure the level of air pollution by using TIR and SWIR bands. Hence, the objective of this research investigation is to extract air pollutant data from satellite images, using high spectral and spatial resolution ASTER band in SWIR and TIR ranges. This to correlate ASTER satellite based measurements, in terms of raster pixel digital numbers, in comparison with the criteria pollutants EPA ground based data. This research can demonstrate the greater potential benefit of ASTER data for the detection of emissions and transport of air pollutants.

Chapter 2

Methods and Techniques

2.1 Study Area

This research investigated three locations, where high pollution concentrations are reported by air quality monitoring agency and general media. These locations are subsequently studied. Firstly San Francisco Bay is a unique land feature, absolutely land
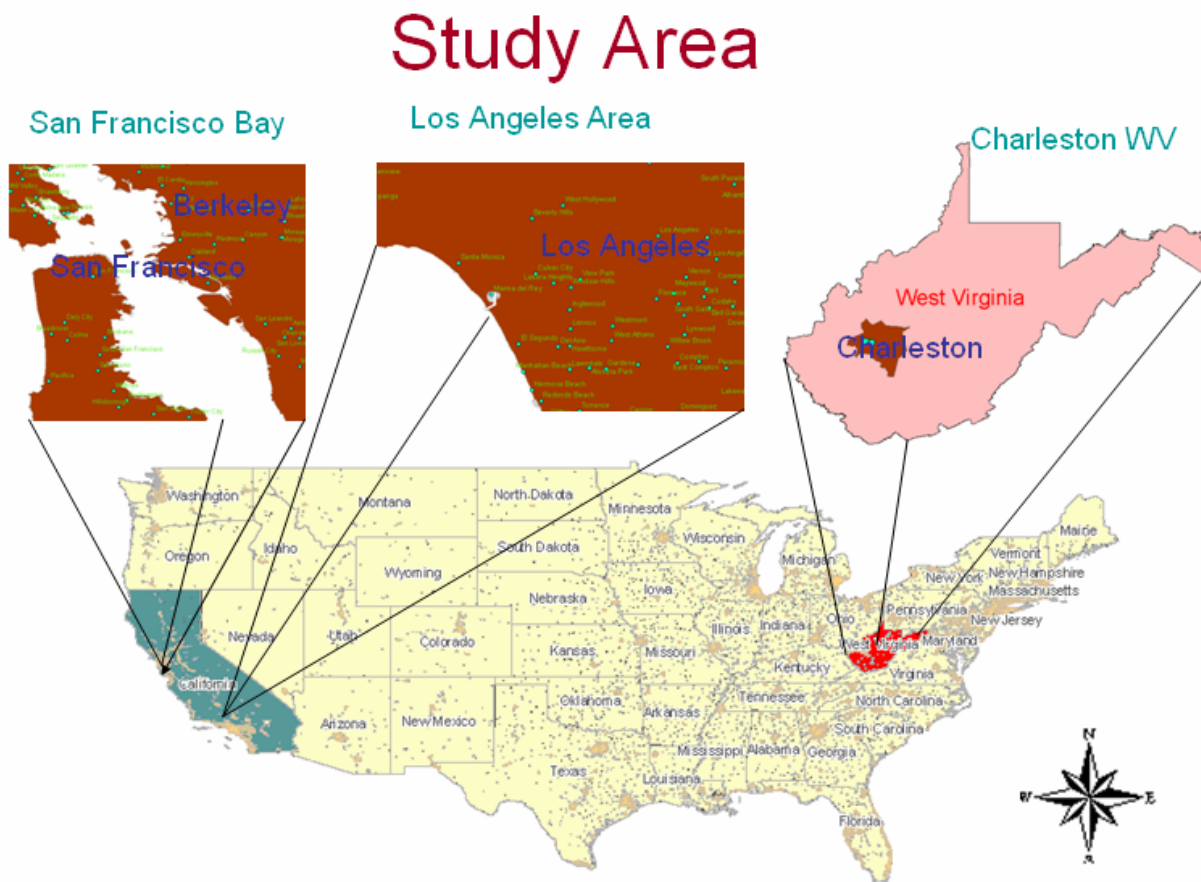
Figure 1: GIS vector map of mainland USA, showing San Francisco Bay Are and, Los Angeles area in California, and Charleston, in West Virginia (WV), created in ESRI ArcGIS 9.1 software.

locked by mountain ranges, although having maritime climatic conditions. Due to rapid industrialization since the Second World War, it has multiple air pollutant sources. In 2000 the Bay area recorded CO and PM $_{10}$ concentrations, exceeded federal standards, by 110% and 117% respectively (South Coast Air Quality Management District, Annual Report, 2000). Also the California Air Resource Board reported prolonged high PM_10 emission, particularly, at Berkeley in the San Francisco Bay Area (cited in Pacific Steel Casting Company's proposed odor control plan report, 2005).

Secondly Los Angeles has been a concern for environmentalists for air pollution since the industrialization that accompanied the Second World War. In the early 1950's Professor Haagen-Smit of the California Institute of Technology demonstrated that a key feature of Los Angeles smog involved photochemical reactions that occur on a mixture of hydrocarbon vapors and oxides of nitrogen, with subsequent formation of aldehydes, HNO_3, peroxy-acyle nitrates (PAN) and particulate matter (PM). Los Angeles contains a number of oil fields, petroleum refineries and power plants that need to supply all of southern California and parts of Nevada and Arizona (UNEP Assessment Report, 2004). In Los Angeles County, Lynwood and Burbank's PM_10 concentrations recorded in the year 2003, exceeded Federal standard for 30 days (California Air Resource Board report, 2003). Los Angeles now is ranked as the most polluted US city (in smog and particulates), by American Lung Association (ALA) 2004 report.

Thirdly Charleston, the capital of West Virginia, is known as the city of chemical industries. It is situated in the Kanawha valley in the mountain state of West Virginia, where there are chemical industries, smelting industries, and two big power plants. Charleston is also

ranked as the sixteenth most polluted city (PM_2.5 species) in USA by the ALA 2005 report.

2.2 Data Acquisition

2.2.1 Satellite Image Sensor's Data

ASTER raw level-1 (L1A) data of Los Angeles (acquired on October 17, 2003 at 10:23 am local time), San Francisco Bay Area (acquired on March 10, 2000 at 10:21 am local time), and Charleston (acquired on September 19, 2005 at 10:26 am local time), WV are collected from the United States Geological Survey (USGS). Satellite images were taken during fairly dry seasons and cloud free condition in order to accurately assess the atmospheric smog.

2.2.1.1 Sensors

Advanced Spaceborne Thermal Emission and Reflection Radiometer (**ASTER**) is an imaging instrument flying on Terra satellite which was launched in December 1999 as part of NASA's Earth Observing System (EOS). It is a cooperative effort between USA's NASA and Japan's Ministry of Economy and Industry (METI) formerly known as Ministry of International Trade and Industry (MITI), with collaboration of scientific and industrial organizations in both countries (ASTER user handbook, JPL, 2000). Terra is orbiting the earth at 705 km altitude, in a sun-synchronous orbit 30 minutes behind the Landsat ETM+. It crosses the equator   at about 10:30 am local solar time. The orbit inclination is 98.3 degrees from the Equator. Orbit time is 98.88 minutes, and ground track repeat cycle is 16 days.

ASTER has 14 bands in the visible and near infra-red (VNIR), the short wave infra-red (SWIR) and the thermal infra-red (TIR).   ASTER is the only high spatial resolution instrument on Terra System; therefore it acts like a 'zoom lens' for the other instruments in Terra. There are three visible and near infra-red (VNIR) bands having 15 m spatial resolution in $0.52\,\mu$m – $0.86\,\mu$m range, six SWIR bands having 30 m spatial resolutions in $1.6\,\mu$m – $2.43\,\mu$m range, and five TIR bands having 90 m spatial resolution in $8.125\,\mu$m-$11.65\,\mu$m range.

The VNIR subsystem of ASTER consists of a 5000 element silicon charged-coupled detector (CCD). In SWIR subsystem, the detector in each of the six bands is a Platinum Silicide-Silicon (PtSi-Si) Schottky barrier linear array. Six optical band pass filters are used to provide spectral separation. The TIR subsystem uses 10 Mercury-Cadmium-Telluride (HgCdTe) detectors in a staggered array with optical band-pass filters over each detector element.

2.2.1.2 Data Type

All data products are stored in a specific implementation of Hierarchical Data Format called HDF-EOS. ASTER L1A data are formally defined as reconstructed, unprocessed instrument data at full resolution. They consist of the image data, the radiometric coefficients, the geometric coefficients, and other auxiliary data without applying the coefficients to the image data, thus maintaining the original data values. ASTER raw level-1 (L1A) data of Los Angeles, San Francisco Bay Area, and Charleston, WV are used in this research in order to accurately assess the atmospheric smog.

2.2.2. Digital Raster Graphics and other GIS Data

Georegistered Digital Orthophoto Quarter-Quadrangles (DOQQ's) and ESRI shapefiles of road network, rivers, and basemap of the respective sites were used in this investigation. DOQQ's and ESRI shapefiles are provided by California Spatial Information Library, Sacramento, CA, and West Virginia GIS Technological Center, Morgantown, West Virginia.

2.2.3. Air Quality Data

Air Quality Monitoring data and facilities emission data has been acquired from the United States Environmental Protection Agency (US-EPA) regional centers. The EPA data consists mainly of NO_x, CO, SO_2, PM namely, PM_10 and PM_2.5. EPA monitoring stations collect air pollutants concentrations on an hourly basis. For this research US EPA provided data on the same day, on an hourly basis, as that of the satellite sensor data acquisition. EPA's facility emission data of Charleston, WV, for the respective years, are also used in this investigation. The air quality standards refer to respirable suspended particulate matter (PM_10). The air quality standards for PM_10 typically range from 10-150 μ g/m^3 are annually averaged depending on particle composition and national legislation. The USA Federal standard for PM_10 is 50 μ g/m^3 and its Hazardous Standard is 150 μ g/m^3. For Carbon monoxide (CO) federal standard is 9.0 Parts per Million (ppm). While that of federal NO_x is 54 ppm, and that for sulfate is 24 μ g/m^3.

2.2.3.1. Air Quality Monitoring Instruments

Currently EPA monitoring stations use particle mass analysis instruments namely, Tapered Element Oscillating Microbalance (TEOM), Continuous Ambient Mass Monitor (CAMM), or Beta Attenuation Method Sampler (BAMS), (EPA and Air resources Board, 2005). The detection technologies employed in particle mass analysis instruments include Beta gauges, piezoelectric crystals and harmonic oscillating elements. These technologies were designed for real-time mass analysis of particles in size ranging up to 10μ m. The sensors use imaging and elemental analysis techniques which provide both morphological and chemical composition information respectively. These are microprocessor-based units which accommodate most of the analysis requirements. These provide internal data storage, advanced analog and serial data input/output capabilities. Nanotechnology based sensors present opportunities to create new and better products for orbital image and ground sensor initiatives. In December 2004, EPA's Science Policy Council (SPC) formed a cross-Agency Nanotechnology Work group for examining potential implication and application of nanotechnology to improve assessment, management, and prevention of environmental risks. Nanotechnology based sensors are nanoparticles and nanotube based devices, where in some cases carbon nanotubes (CNTs) connect two metal electrodes and conductance between them is observed as a function of gate bias voltage (Vaseashta and Irudayaraj, 2005). Since electrical characteristics are influenced by the atomic structure, any change such as mechanical deformation and chemical doping, induce change in conductance, thus rendering such devices sensitive to their chemical and mechanical environment (Vaseashta and Irudayaraj, 2005) Nanostructured based sensors have lower material costs, reduced weights

and power consumption of the sensors (Vaseashta et al, Springer, 2005). Nanotechnology offers the potential to improve exposure assessment by facilitating collection of a large number of measurements at a lower cost and improved specificity (Vaseashta et al, 2006).

2.2.4. Climatic Data

For this investigation, Wind speed, direction, precipitation and humidity data of San Francisco Bay area, Los Angeles area, and Charleston are collected from National Oceanic and Atmospheric Administration (NOAA) - National Climatic Data Center, Reno, Nevada. The climate data gave appropriate information about possible transport of pollutants to longer distances.

2.3. Data Processing

2.3.1. Satellite Data Processing

ASTER L1A raw data, of the respective sites, has been geometrically corrected and geo-registered in Universal Transverse Mercator (UTM) coordinate system, and WGS84 datum, by image-to-image registration process with DOQQ in ER-Mapper 7.1 software. Georegistered ASTER images are combined with respective DOQQs by the Data Fusion (DF) technique in ER-mapper 7.1 software. The Principal Component Analysis (PCA) Technique has been applied to extract atmospheric smog in the imagery in ER-Mapper 7.1 software. Density Slicing (DS), Band Ratioing (BR), and Spatial Filtering (SF) techniques are also employed to enhance atmospheric pollutants in the imagery in ER-mapper 7.1 software.

2.3.1.1. Data Fusion

Data fusion is the combination of multi source data, having different characteristics such as spatial, spectral and radiometric characteristics, to acquire high quality image. The integration of spectrally and spatially complementary remote multisensor data facilitates visual and enhanced image interpretation (Jensen, J. Prentice Hall, 2005). To effectively utilize the high spectral resolution and moderate spatial resolution ASTER images, data fusion techniques has been applied, with the high spatial resolution of 1 meter DOQQ's, using ER-Mapper 7.1 software. It effectively combines multi source images into one composite color image of greater quality and preserved spectral characteristics whilst increasing spatial resolution of images.

2.3.1.2. Principal Component Analysis

The PCA technique involves a mathematical procedure for simplifying a dataset by reducing multidimensional datasets to lower dimensions by analysis. It transforms a number of (possibly) correlated variables into a (smaller) number of uncorrelated variables called principal components (PC). PC axes and bands of ASTER can be presented in a covariance matrix with highest variability in the image data loaded in the first PC axis and the least in the last PC axis (Jensen, 2003). The PCA algorithm function uses each image band as a variable and rotates the multivariable axes about the statistical grand mean from the image dataset. This transforms the data axes to maximize the variability in the first PC (PC1) with the each successive component of the variability, such as second PC (PC2) and so on, loaded into each successive axis orthogonal to the previous axis (Figure 2). The first principal component
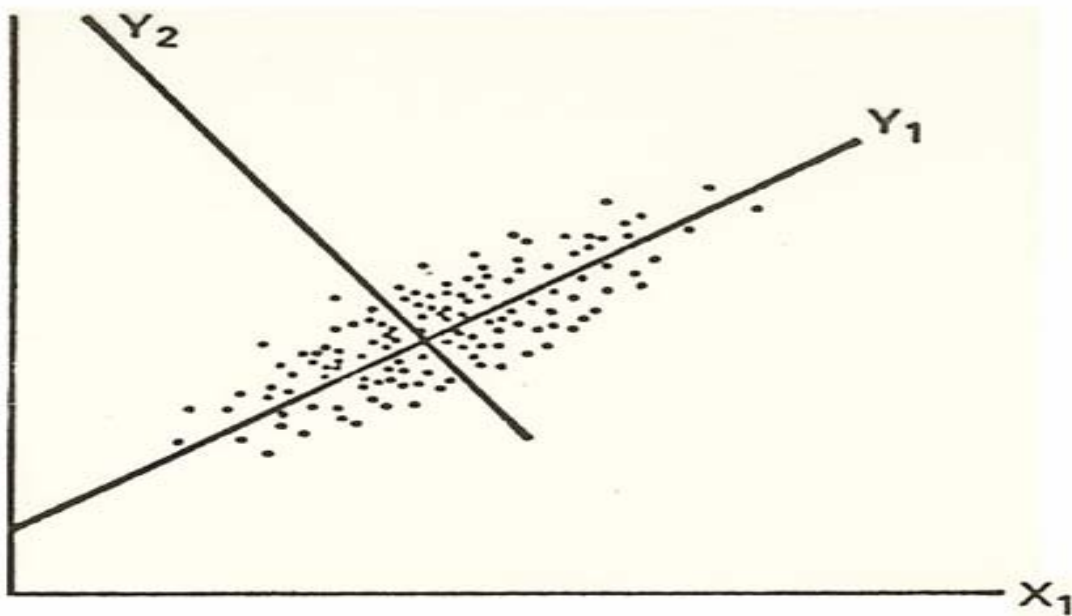
Figure 2: Principal Component Analysis: Rotation of data swarm axis about statistical grand mean of each axis (band). Resultant data acquires more variability.

accounts for as much of the variability in the data as possible, and each succeeding component accounts for as much of the remaining variability as possible. This maximizes the supportability of the feature and enhances the features for extraction and pattern recognition in the image (Brumfield et. al, 1991). In order to extract features in the image data set PCA technique has been applied in 1-14 bands of the resultant images (with DOQQ as an intensity layer). Red green and blue (RGB) color composites images are made using PC1, PC2, and PC3.

2.3.1.3. Density Slicing

Density slicing is a form of selective one-dimensional classification. The continuous pseudocolor scale of the resultant image is "sliced" into a series of classifications based on ranges of brightness values. All pixels within a "slice" are considered to be the same information class. This method is especially useful when a given surface feature has a unique and generally narrow set of digital number (DN) values (Jensen, J. 2005). Density slicing technique has been applied on the resultant dataset in band 14 for HNO_3 absorption band at 11 μm, band 7 for Carbon monoxide and carbonate absorption band at 2.3 μm, band 5 for cirrus cloud (ice crystal) absorption band at 2.1 μm, and band 4 for water vapor absorption band at 1.67 μm.

2.3.1.4. Band Ratioing

Band Ratioing is a process by which brightness values of satellite image pixels in one band are divided by the brightness values of their corresponding pixels in an another band in order to create an enhanced new output image. This technique is useful when there are subtle differences in signature of features in the dataset (Jensen, 2005, Prentice Hall). In this investigation band ratioing technique was found necessary only in Charleston area where all other image processing techniques were unable to distinguish cloud properties, and atmospheric pollution signatures.

2.3.1.5. High-pass Spatial Filtering

High-pass filtering is a digital technique based on a convolution process. A filter is defined by a kernel, which is a small array applied to each pixel and its neighbors within an image. The convolution may be applied in either the spatial or frequency domain. Within the spatial domain, the first part of the convolution process multiplies the elements of the kernel by the matching pixel values when the kernel is centered over a pixel. The elements of the resulting array are averaged, and the original pixel value is replaced with this result. A high pass filter tends to retain the high frequency information within an image while reducing the low frequency information. This enhances the interfaces among features, and can be used to distinguish features in the atmosphere.

2.3.2. In-situ Data Processing

EPA air quality pollutants concentration data in tabular form has been converted into a .dbf files of dBase 4 in Microsoft Excel worksheet, and loaded into ESRI ArcGIS 9.1 software. This point feature is used to locate the monitoring stations in DOQQ's and the image dataset from the respective sites. These monitoring stations are then located in the ASTER processed imagery to find the reflectance digital numbers of the respective monitoring station pixel values in order to find correlation with EPA monitoring data.

Chapter 3

Results and Discussion

3.1. Study Area I: San Francisco Bay Area:

Accurate knowledge of spatial distribution of the atmospheric pollutants over a city is currently very difficult due to limited number of monitoring stations. A GIS map of EPA

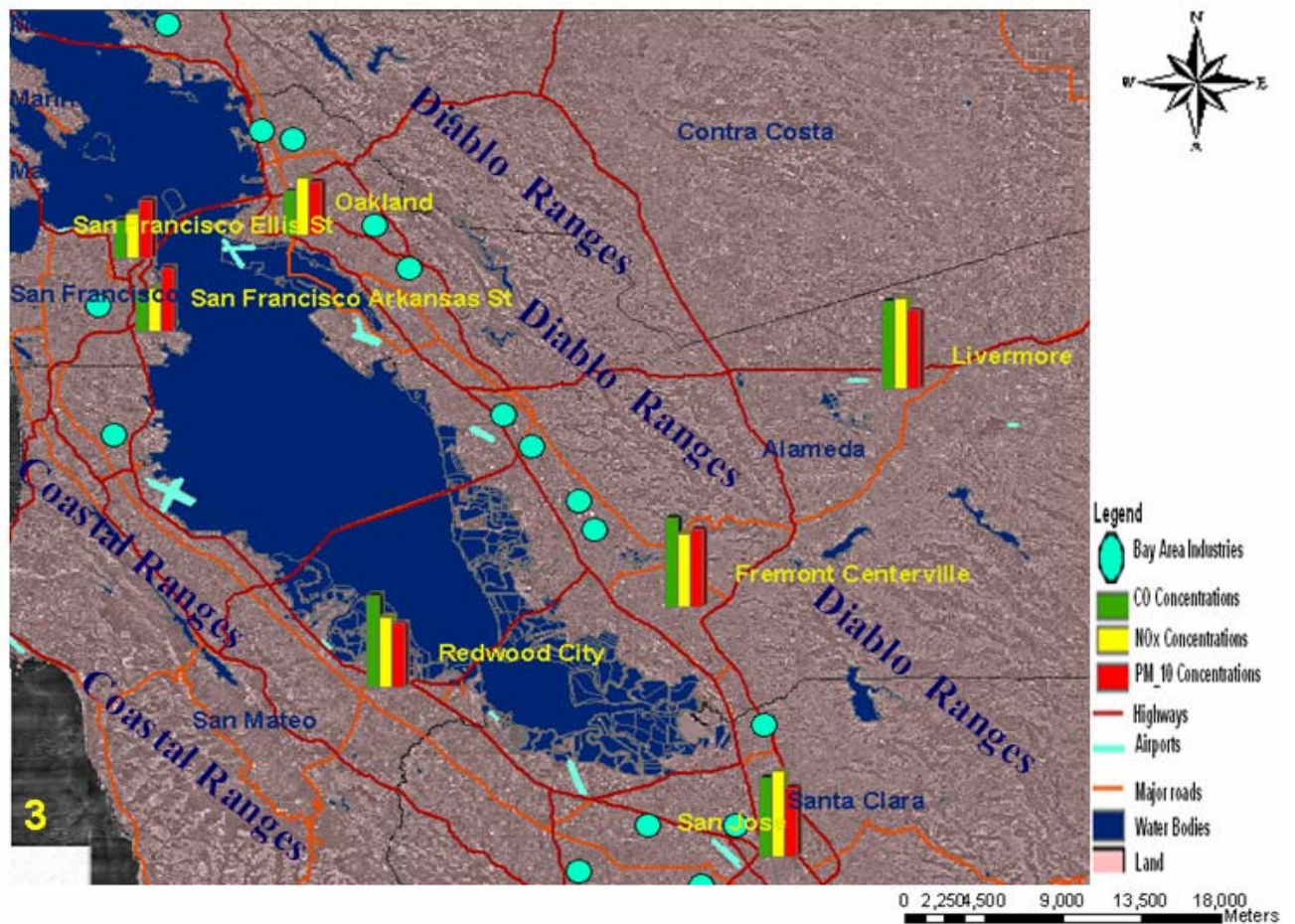*Figure 3: GIS map of industries location and EPA Air quality Monitoring Pollutant concentrations measured at 6:00am on the day of satellite data acquisition on March 10, 2000 in the San Francisco. EPA monitoring concentrations of CO are shown in green, NOx in yellow, PM_10 in red bar graphs. Industry location information is provided by South Coast Air Quality Management District data and California Air Resources Board data, 2005.*

monitoring stations (Figure 3) in San Francisco Bay area created in ESRI ArcGIS 9.1 software, shows limited opportunity to assess air pollutant from in-situ data provided by EPA. The data for CO in EPA monitoring stations shows relatively high concentration in Redwood City (4.4 ppm), Fremont (4.2 ppm), and the San Jose (3.8 ppm) area, but is much below the hazardous health related standard of 9.0 ppm (EPA, 1998). Remote Sensing of CO has been achieved in TIR using the absorption band at 4.6 μm and in SWIR at 2.3-2.34 μm (Maziere M. De et al. 2005). The data for PM_10 (Figure 3) in EPA monitoring stations in the San Francisco Bay area show that the PM_10 concentrations in Fremont (54ppm), Livermore (54ppm), and San Jose (48ppm) had high concentrations at early morning hours. NOx concentration was found highest at Freemont (0.383 μg/m^3, followed by San Jose (0.361 μg/m^3) at early morning hours. The facilities data provided by South Coast Air Quality Management District data and California Environment Protection Agency, Air Resources Board, October, 2005 report shows that there are multiple air pollutant sources in the Bay area.

Climatic condition data monitored on March 10, 2000, from the NOAA National Climatic Data Center data, are shown in ASTER RGB 14-7-2 bands in Figure 4. There were variable wind patterns existing during morning, afternoon, evening and night periods (note Figure 4).
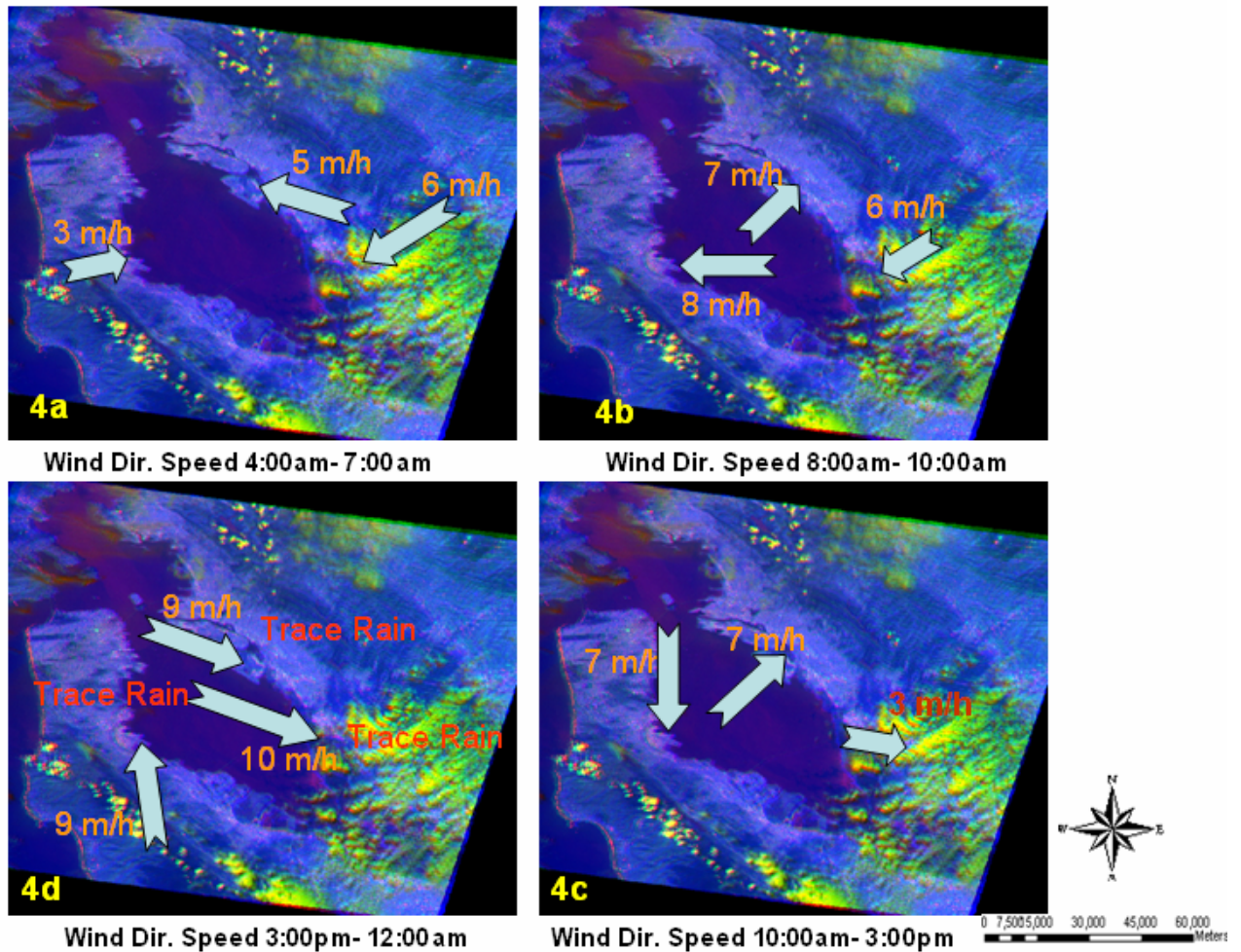
Figure 4: Wind pattern on March 10, 2000 at San Francisco Bay area shown in four time intervals. a) 4:00 am -7:00 am, directed towards the bay. b) 8:00am -10:00am directed towards land, except at Fremont, directed towards bay. c) 3:00 pm-midnights: directed towards SE, except at San Francisco where it is towards north. (d) 10:00am-3:00pm directed towards land in all the three monitoring stations.

ASTER datasets acquired on March 10, 2000, at local time 10:31 in the San Francisco Bay Area are processed according to the methods mentioned before in this manuscript. PCA image bands 1-14 of March 10, 2000 (Figure 5a) show, cloud patterns in different tones of blue in the San Francisco Bay area atmosphere, but the PCA image of bands 1-9 (Figure 5b) does not show different tones in pink. The Density sliced image in pseudo color with DOQQ

21
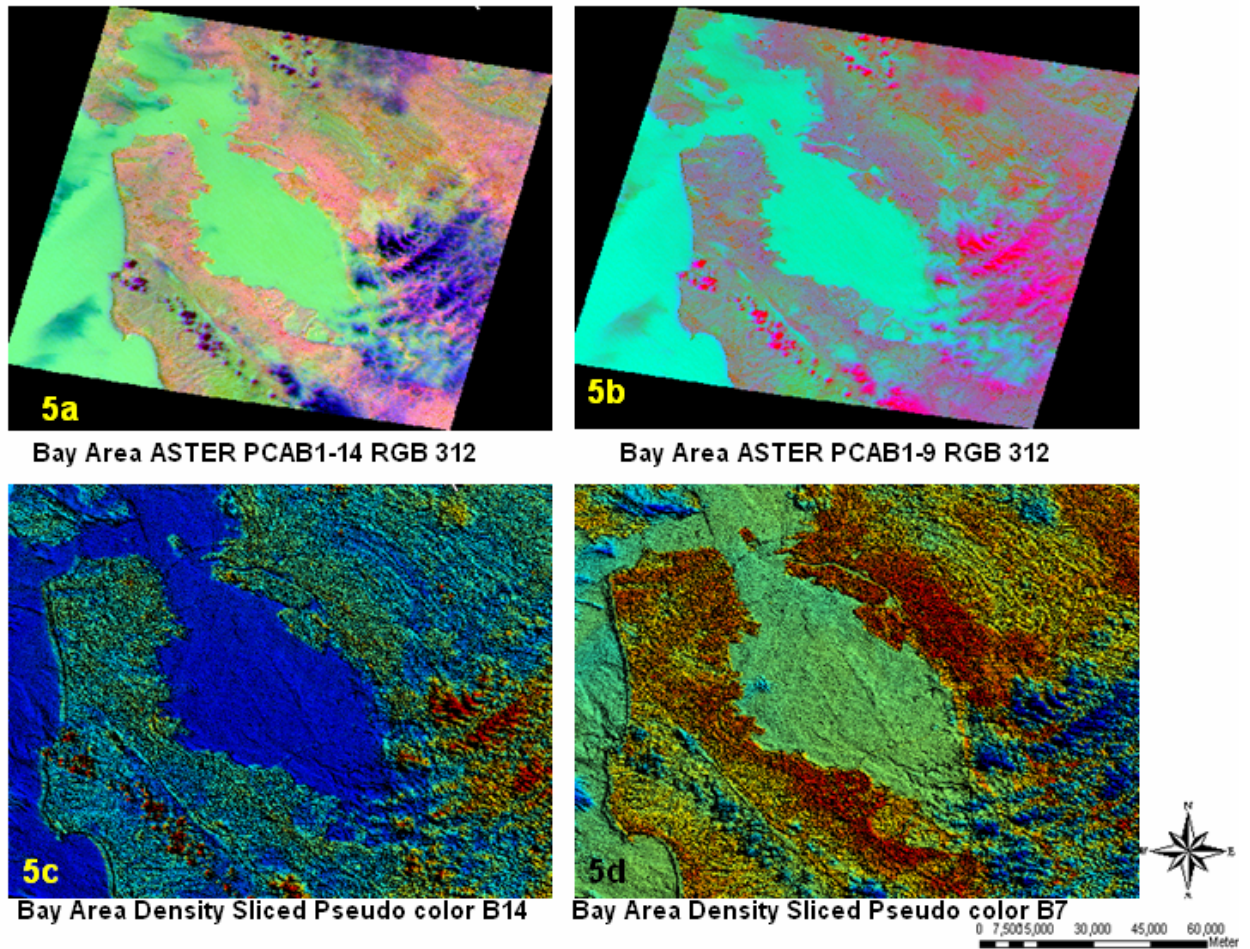
Figure 5: March 10, 2000 San Francisco Bay area ASTER processed images: a) PCA images in all 14 bands. b) PCA image B-1-9 bands. c): Density sliced band 14. d): Density sliced band 7.

as intensity layer in Figure 5c, displays different tones of brown, due to absorption in band 14 (HNO_3 absorption band), but in band 7 (carbonates absorption band), in Figure 5d, the cloud patterns do not show different tones in blues very clearly.

Spectral signatures of freshly emitted industrial pollutants, in all SWIR bands 4-9, and all TIR bands 10-14, are detected by a traverse technique (Roy et. al., 2006) in ER-Mapper 7.1 and compared (Figures 6a and 6b).
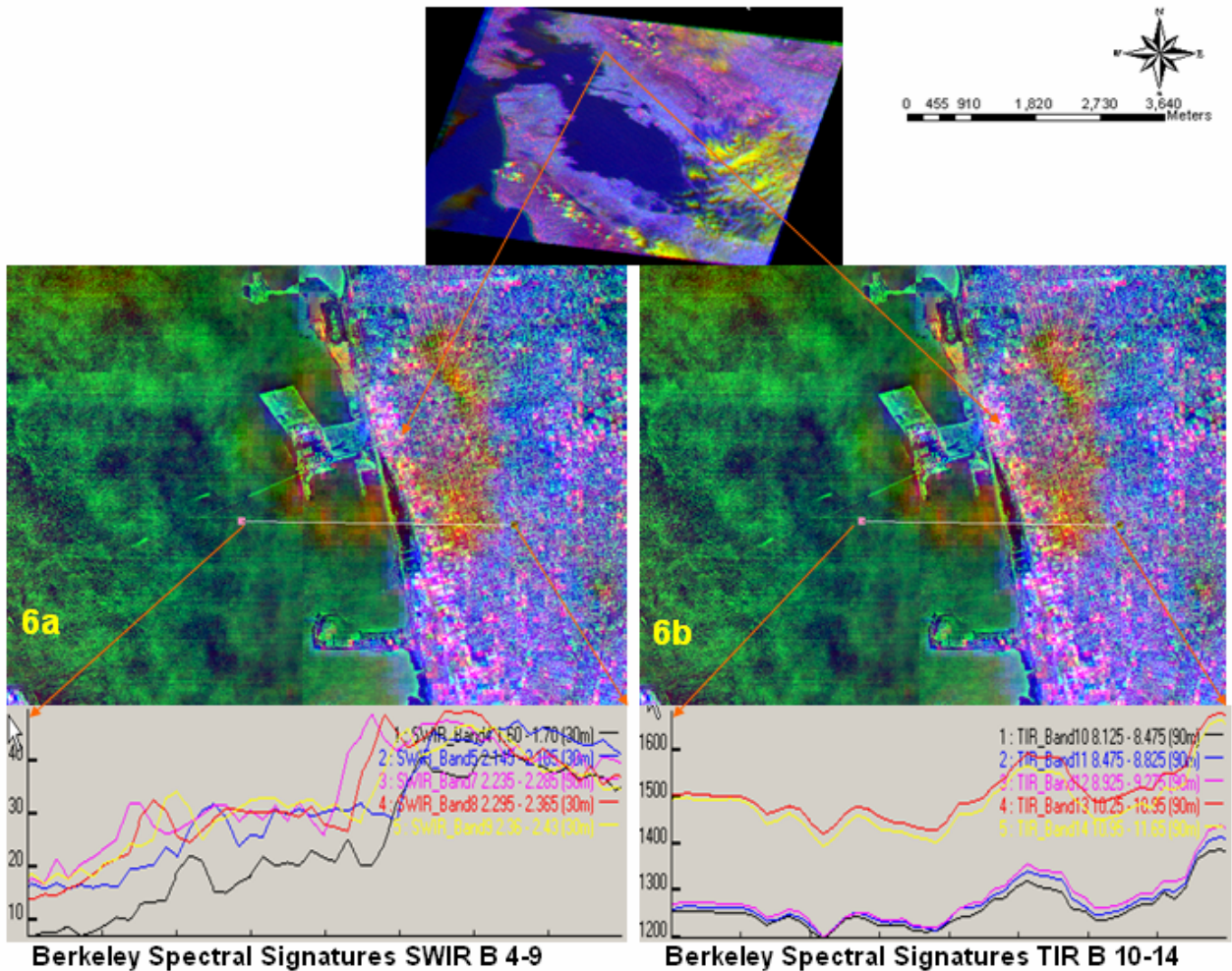
Figure 6: Spectral signatures of freshly emitted air pollutant over a steel casting company in Berkeley, in San Francisco Bay area: a) All SWIR B-4-9 compared, shows variations in absorption. b) All TIR bands B-10-14 compared shows variations in absorption.

Figures 6a and 6b show spectral signatures of freshly emitted air pollutant over a steel casting company in Berkeley area in the ASTER image. It is observed in the Figures 6a and 6b that the SWIR band 7 behaves abnormally compared to other bands. Spectral signatures, of TIR bands 10-14 (Figure 6b) shows almost similar behavior except bands 10 and 14 where more absorption is observed. TIR bands 14 and 10, at 11.0 μ m and 9.0 μ m, are associated with HNO_3 and Methanol absorption band respectively.

In view of observed slight differences in spectral signatures in band 7, a band ratio image composite is created of the ASTER image of the Bay area, with red band ratioed as 14/10 , green band ratioed as 3/5 and blue band ratioed as 3/2.

Bay Area Band Ratio Image RGB Bands 3-2,7-5,14-10
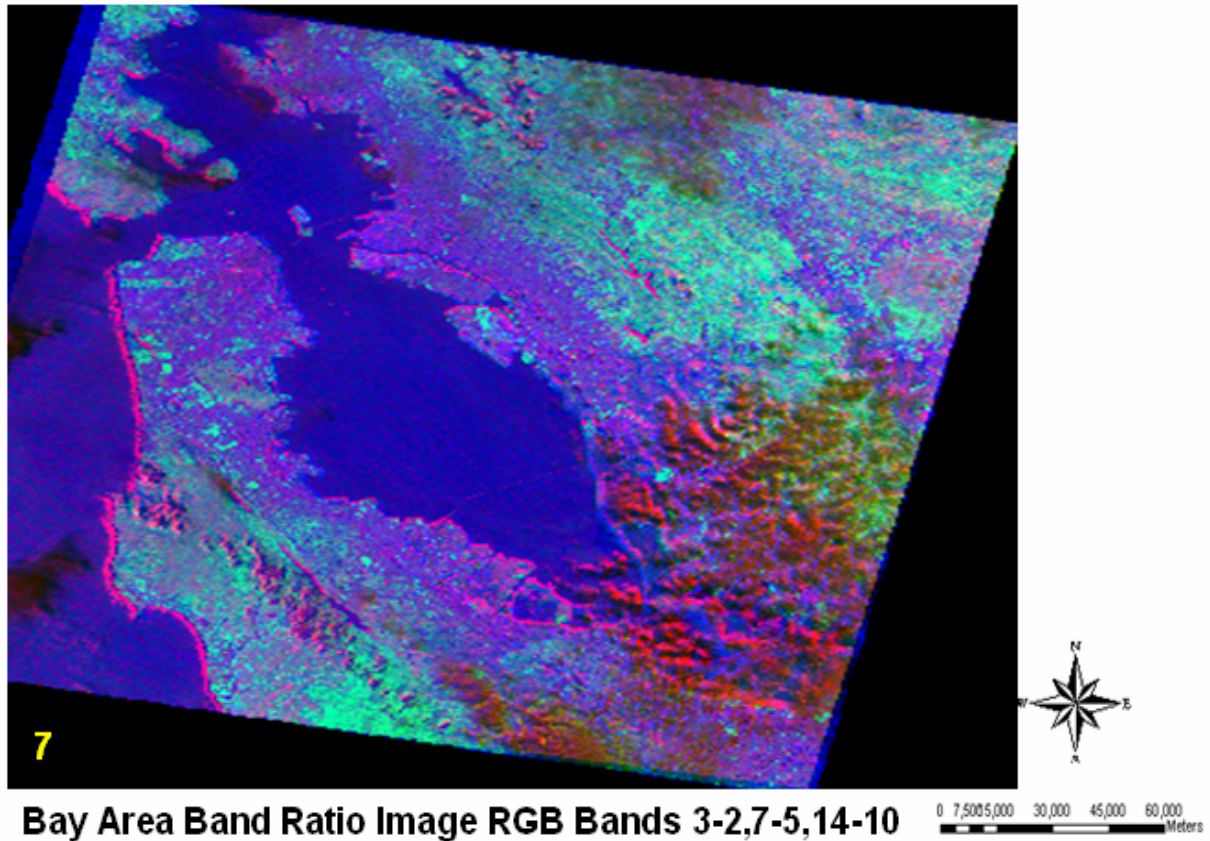
Figure 7: Band ratio composite image in RGB bands 3/2, 7/5, 14/10 of San Francisco Bay area separates regular cloud and suspected pollutants in the cloud pattern.

The resultant image (Figure 7) clearly distinguished regular cloud patterns with atmospheric pollutants in different tones of red and brown.

3.2. Study Area Los Angeles:

The GIS map of Los Angeles area (Figure 8) is created in ArcGIS 9.1 software. The DOQQ is used as a base map, overlaid in ESRI ArcGIS 7.1 software, with Los Angeles area county boundary, highways, water body and airport ESRI shapefiles. EPA monitoring concentrations of CO are shown in green, NOx in yellow, PM_10 in red bar graphs. Industry location information is provided by the EPA and California Air Resources Board data, 2005.
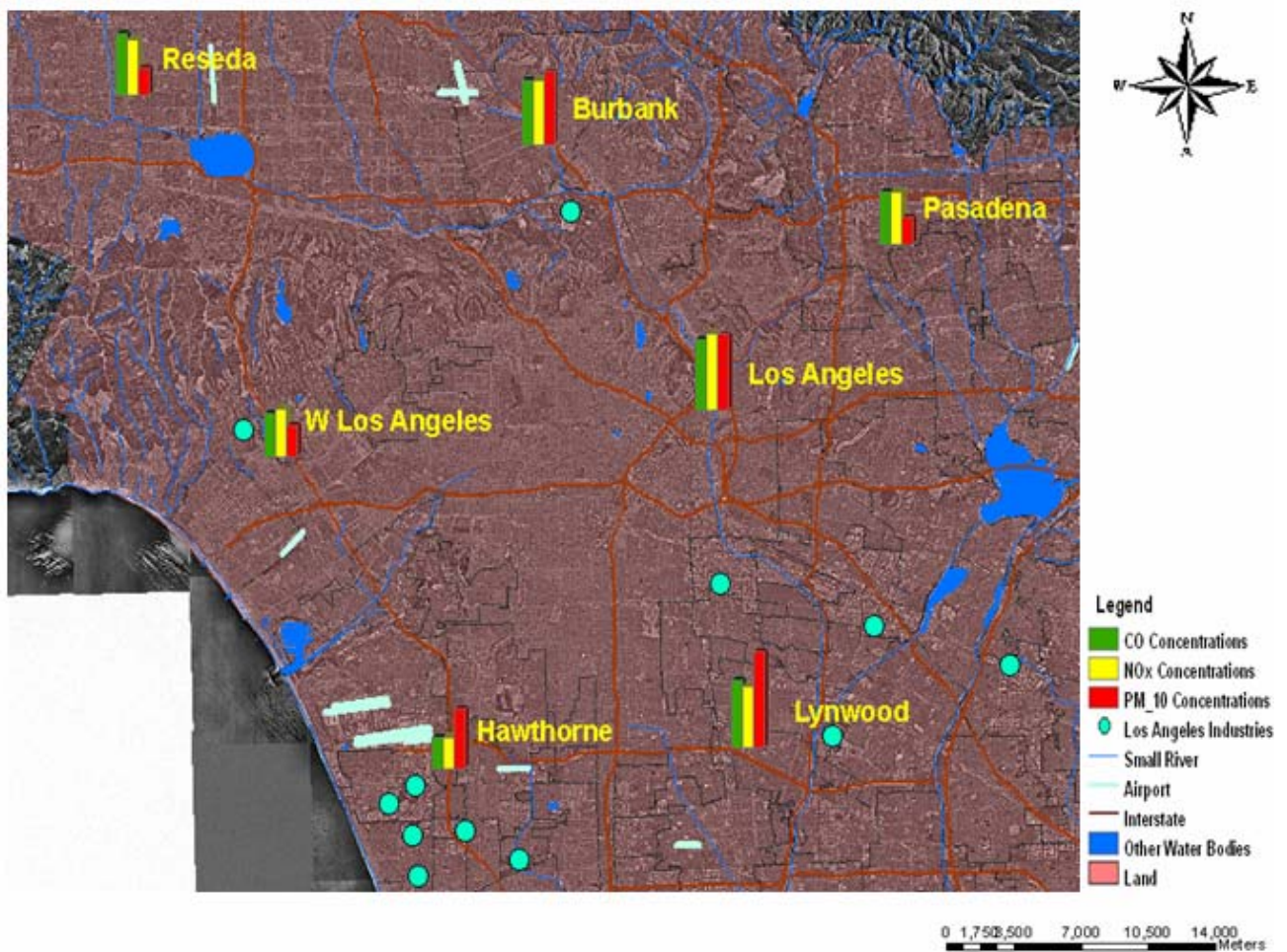
Figure 8: GIS map of industries location and EPA Air quality Monitoring Pollutant concentrations measured at 6:00am on the day of satellite data acquisition on October 17, 2003 in the Los Angeles area. EPA recorded concentrations of CO are shown in green, NOx in yellow, PM_10 in red bar graphs. Industry locations are shown in light blue.

The GIS map of Los Angeles shows that among all of the seven locations in the dataset, the Lynwood (4.6 ppm) area had fairly high CO concentration. The NO_x concentration was highest in the downtown Los Angeles (0.34 μg/m^3) followed by Lynwood (0.33 μg/m^3). It is also observed that PM_10 concentration on October 17, 2003 in Lynwood was extremely high at 121 ppm. Industries locations in the image also suggest that there are multiple sources of air pollution in the area.

The wind pattern data collected from NCDC of NOAA is shown in ASTER image,
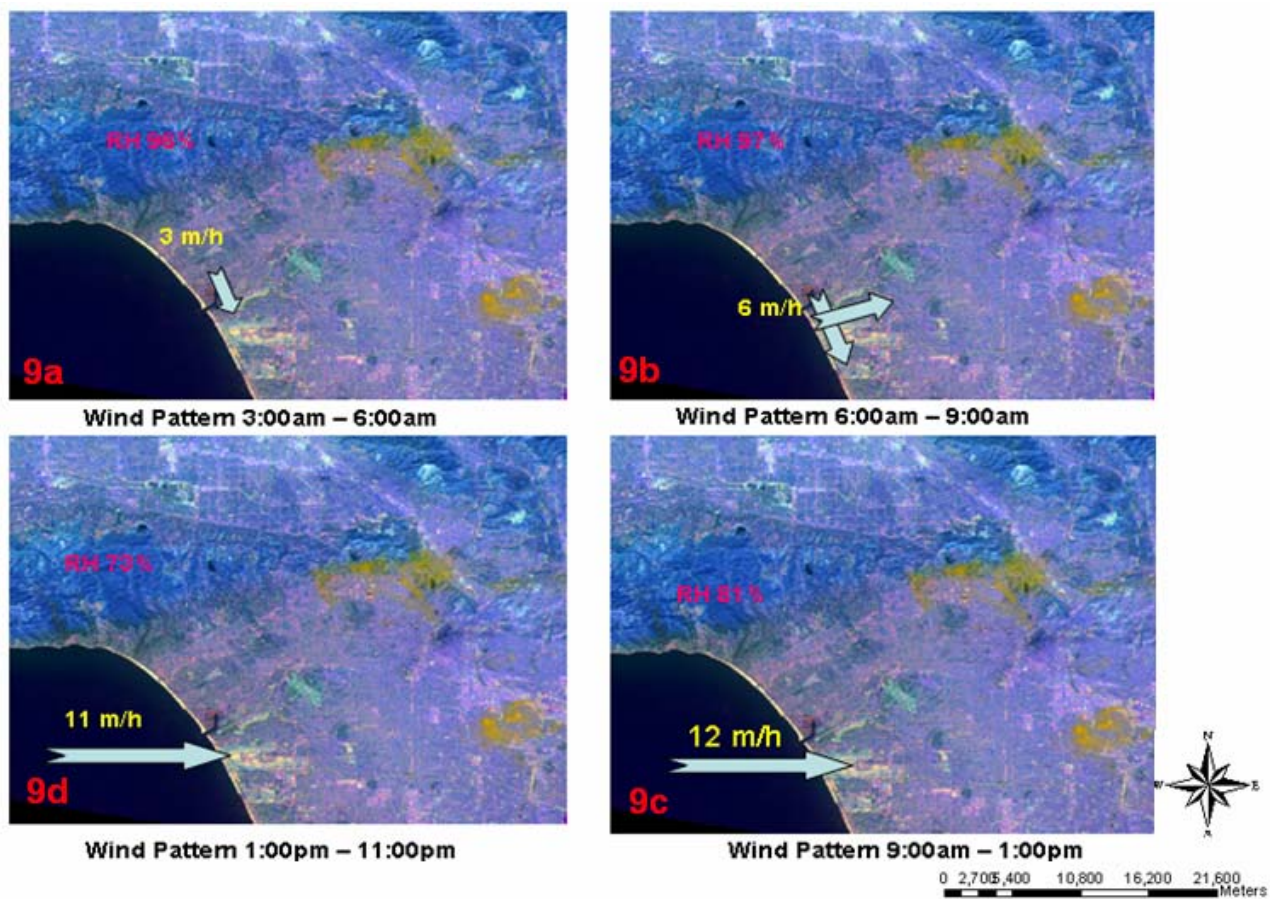
Figure 9. Wind pattern on October 17, 2003 in Los Angeles area: (a) early morning till 6:00am blowing almost southward. (b) 6:00am-9:00am variable winds. (c) 9:00am-1:00pm high speed wind from west. (d) 1:00 pm-midnights also from west.

acquired on October 17, 2003, of Los Angeles area on false color image in RGB bands 14-7-2 (Figure 9). It shows that there were variable wind patterns during midnight till morning and there after blew towards land. High relative humidity and mixing of pollutants by variable winds may cause transport of air pollutants from their source to long distances.

The PCA image bands 1-14 of October 17, 2003 (Figure 10a) shows cloud patterns in
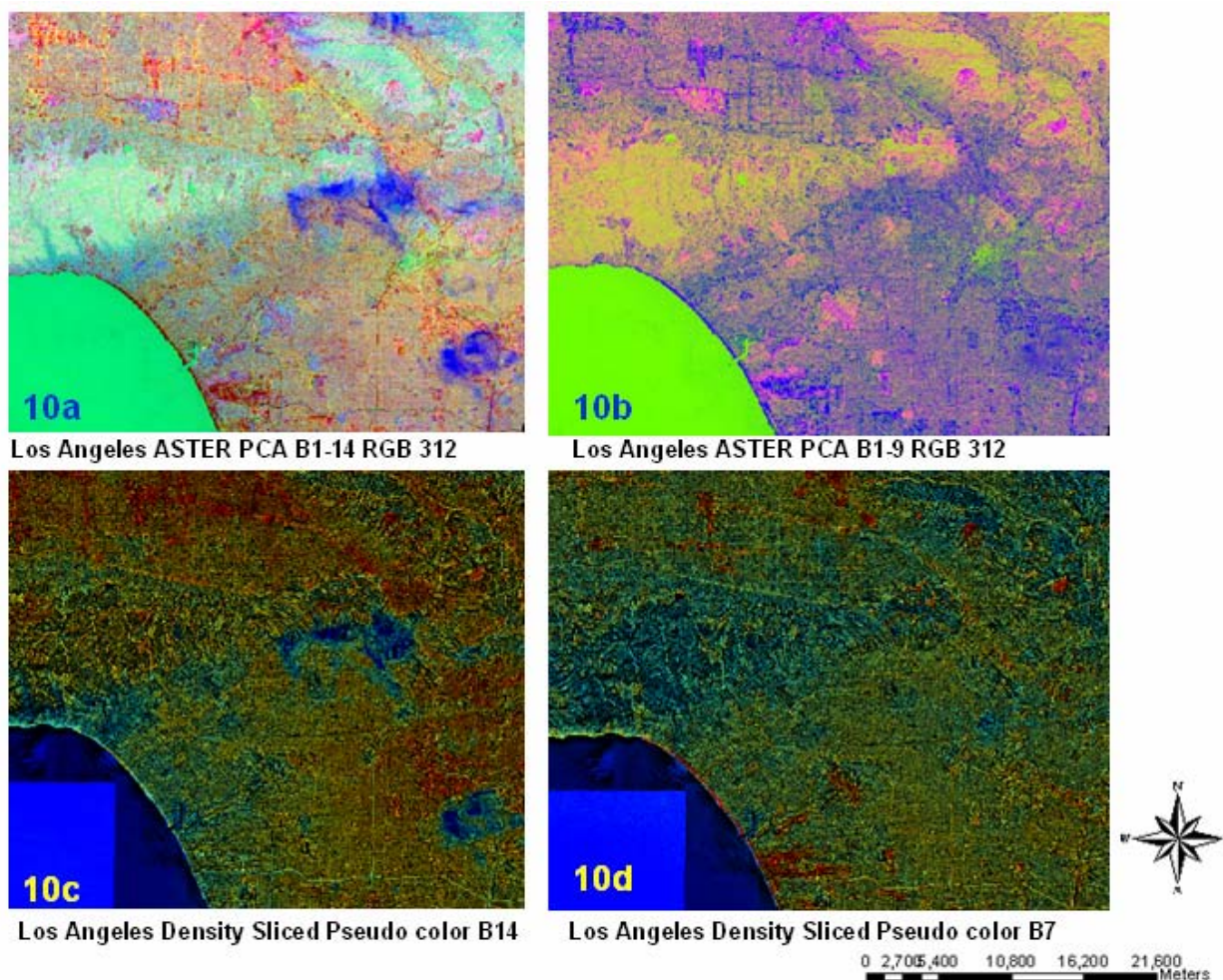
Figure 10: October 17, 2003 Los Angeles area ASTER processed images: (a) PCA images in all 14 bands. (b) PCA image B-1-9 bands. (c): Density sliced band 14. (d): Density sliced band 7.

different tones of blue in the atmosphere of Los Angeles area, but the PCA image of bands 1-9 (Figure10b) is unable to show any cloud pattern. Similar phenomenon observed in the

density sliced image in pseudo color with DOQQ as intensity layer in band 14 (HNO_3 absorption band) Figure 10c, where cloud patterns are shown in different tones of blue, but in band 7 (carbonates absorption band), the density sliced image (figure 10d), the cloud patterns are not observed.

Spectral signature in the entire industrial belt in Commerce and Lynwood area is obtained by traversed technique in ER-Mapper 7.1 software is shown in Figure 11. The SWIR
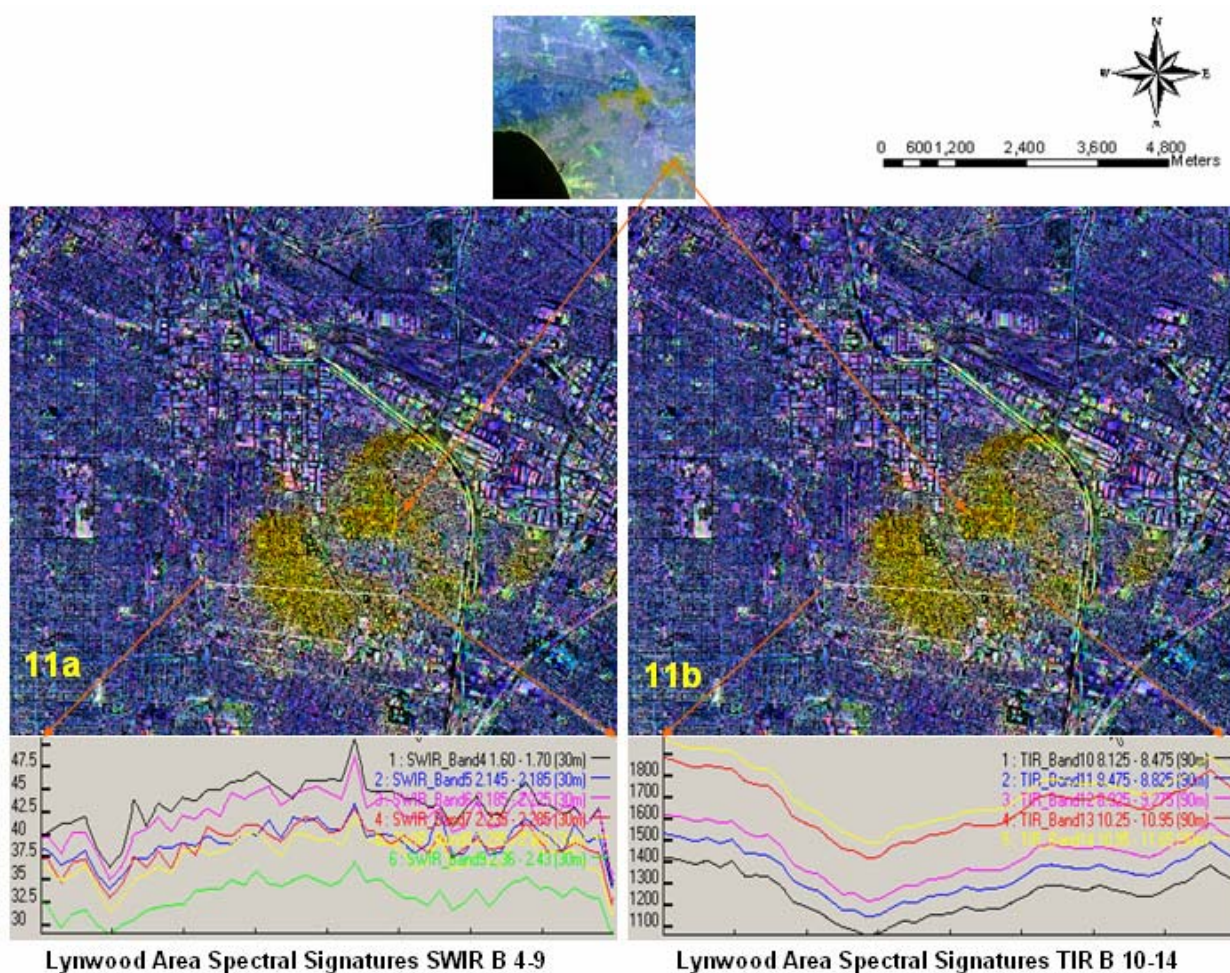
Figure 11: Spectral signatures of air pollutant over Lynwood in Los Angeles area: (a) All SWIR B-4-9 are compared, shows variations in absorption. (b) All TIR bands B-10-14 are compared shows variations in absorption.

bands 9 and 5 behaves in a different way than other SWIR bands (Figure 11a), but it shows strong absorption in all ASTER TIR bands 10-14 (Figure 11b).

The Band Ratio image of Los Angeles area (Figure 12) shows patterns, in different tones of blue throughout the image. It was unable to distinguish regular cloud patterns and other land and atmospheric features. Even the ocean water is also shown in blue. Therefore band ratio image in this particular band combination of 3/2 7/5, 14/10 in RGB is not giving much information about atmospheric pollution in Los Angeles area.

Los Angeles Area Band Ratio Image RGB Bands 3/2,7/5,14/10
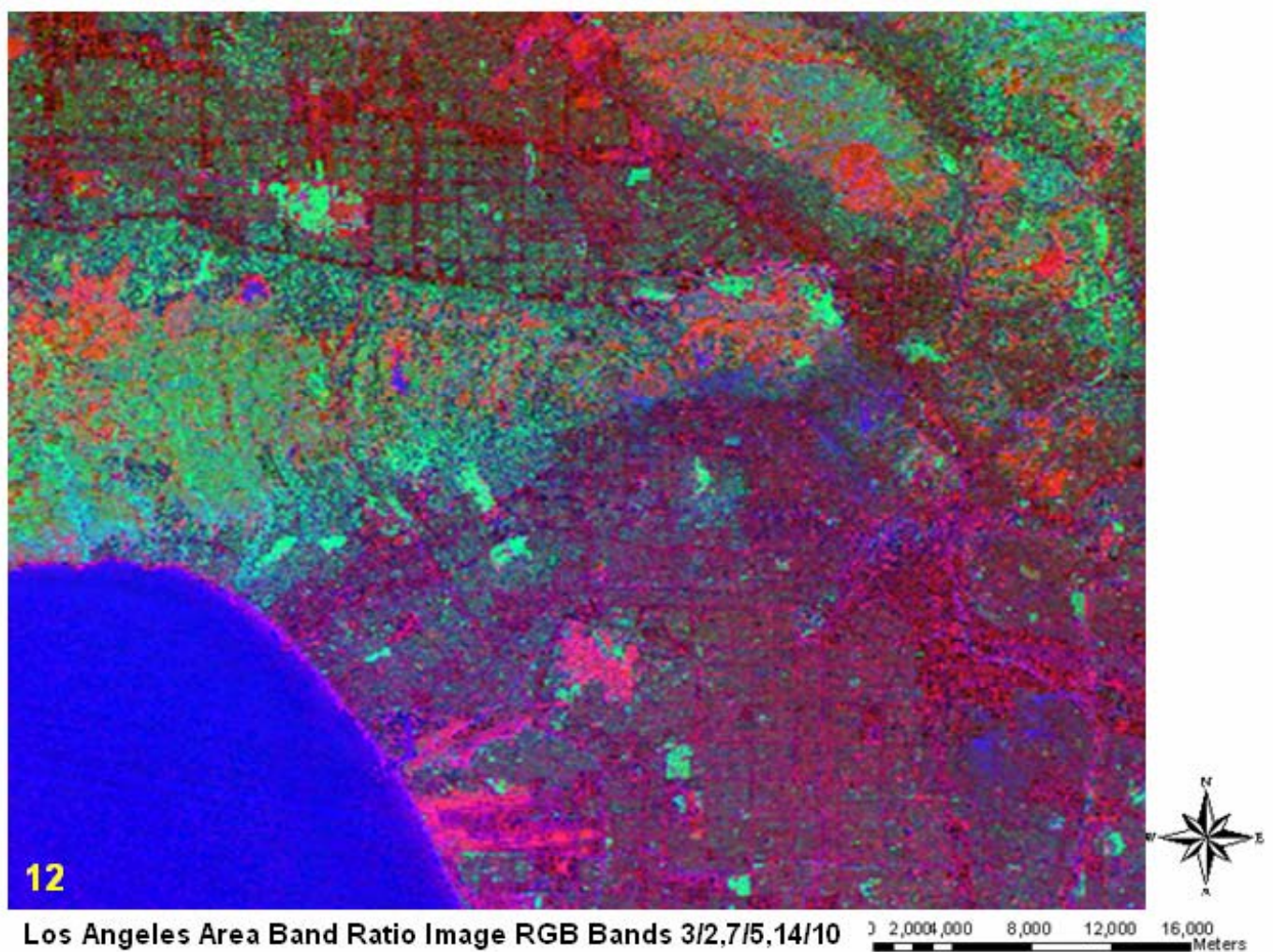
Figure 12: Band ratio image in RGB bands 3/2, 7/5, 14/10 of Los Angeles area unable to highlight plume over the city.

29

3.3. Study Area Charleston:

GIS map of Charleston (fig. 13a) is created in ERSRI- ArcGIS 9.1 software with DOQQ's as a base map, overlayed with highways, railroads, EPA monitoring data and industry shapefiles. It shows EPA monitoring stations recorded very high concentration of NO_X in South Charleston (0.212 ppm federal standard is 0.54 ppm) on the day of satellite
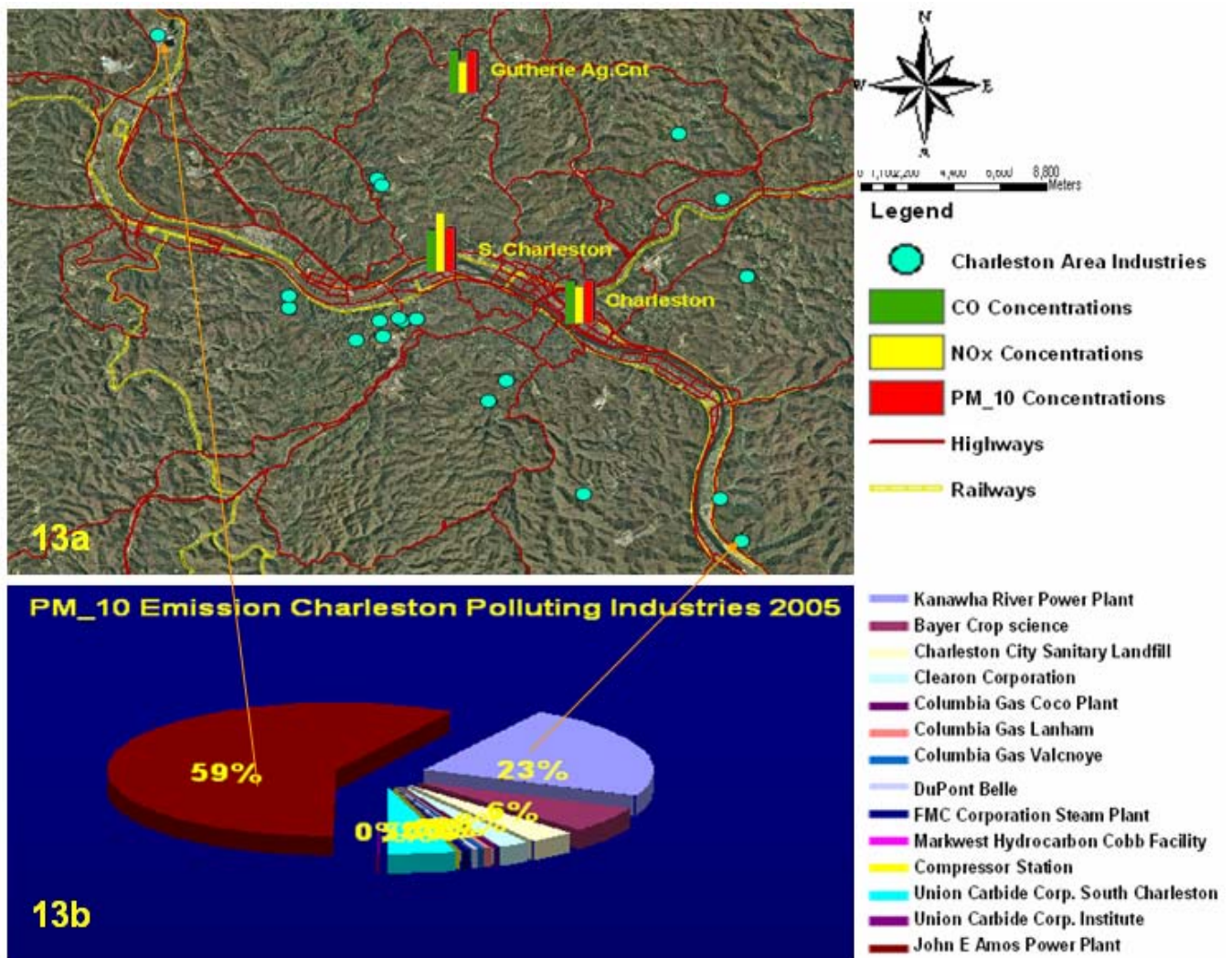
Figure 13: (a) Charleston EPA monitoring station locations in DOQQ, created in ArcGIS 9.1 showing CO, NOx, and PM_10 concentration level on September 19, 2005. (b) Industrial facilities PM_10 annual emission 2005 (Source WVDEP, Charleston).

data acquisition, high concentrations of PM_10 in all EPA monitoring stations (very near to federal high standard of 50 μ g/m^3). Facilities annual emission data from WVDEP (Figure 13b), shows that a substantial part of PM_10 emitted by all the industries in Kanawha valley is emitted by John E. Amos Power plant (59%) and Kanawha River power plant (23%). Most of the industries shown in Figure13a, Charleston area, emit toxic chemicals such as Vinyl Chloride, Methylene Chloride, Benzene, CCl4, in addition to common industrial pollutants like Acetaldehyde, Benzene, Formaldehyde etc (WVDEP, 2005 Report).

Wind patterns on September 19, 2005 in Charleston as recorded by NOAA monitoring station shows the day was calm since early morning till 3:00pm, and thereafter wind was blowing at 7miles per hour from the west (Figures 14a and 14b).

Charleston Wind Dir. Speed 3:00am- 2:00pm
Charleston Wind Dir. Speed 3:00pm-Midnight
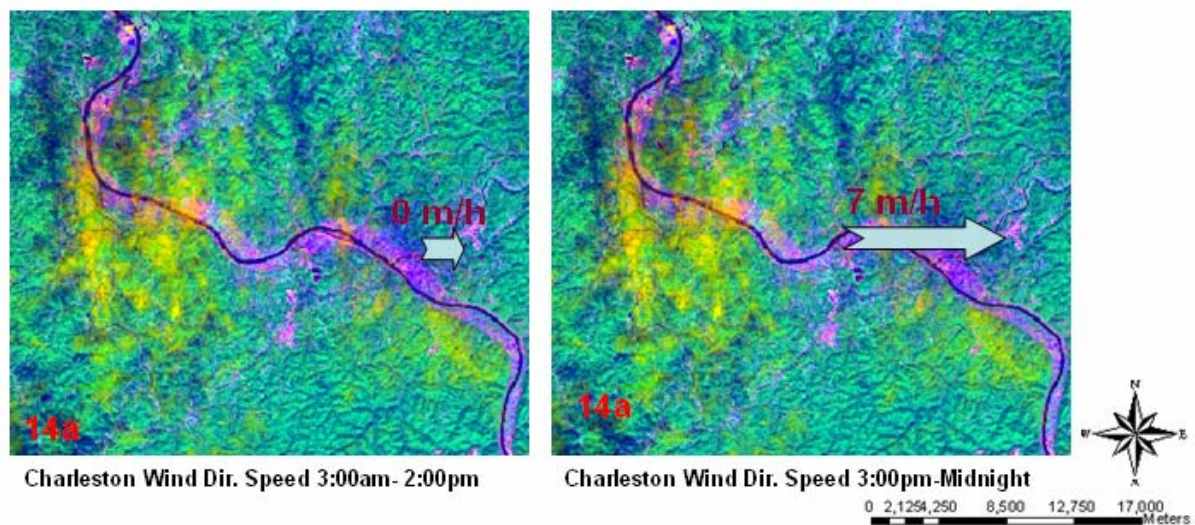
Figure 14: Wind pattern and speed on September 19, 2005, in Charleston area, recorded at NOAA weather station at Charleston airport (NOAA National Climatic Data Center, 2005).

PCA is applied with all ASTER bands (Bands 1-14) as well as with VNIR and SWIR bands (B-1-9). In resultant images, the cloud mask over the city behaves in a similar way

(Figure 15a and 15b). Also density sliced images in ASTER bands 14 and 7 show very little

differences in cloud pattern in different tones of brown (Figure15c and 15d).
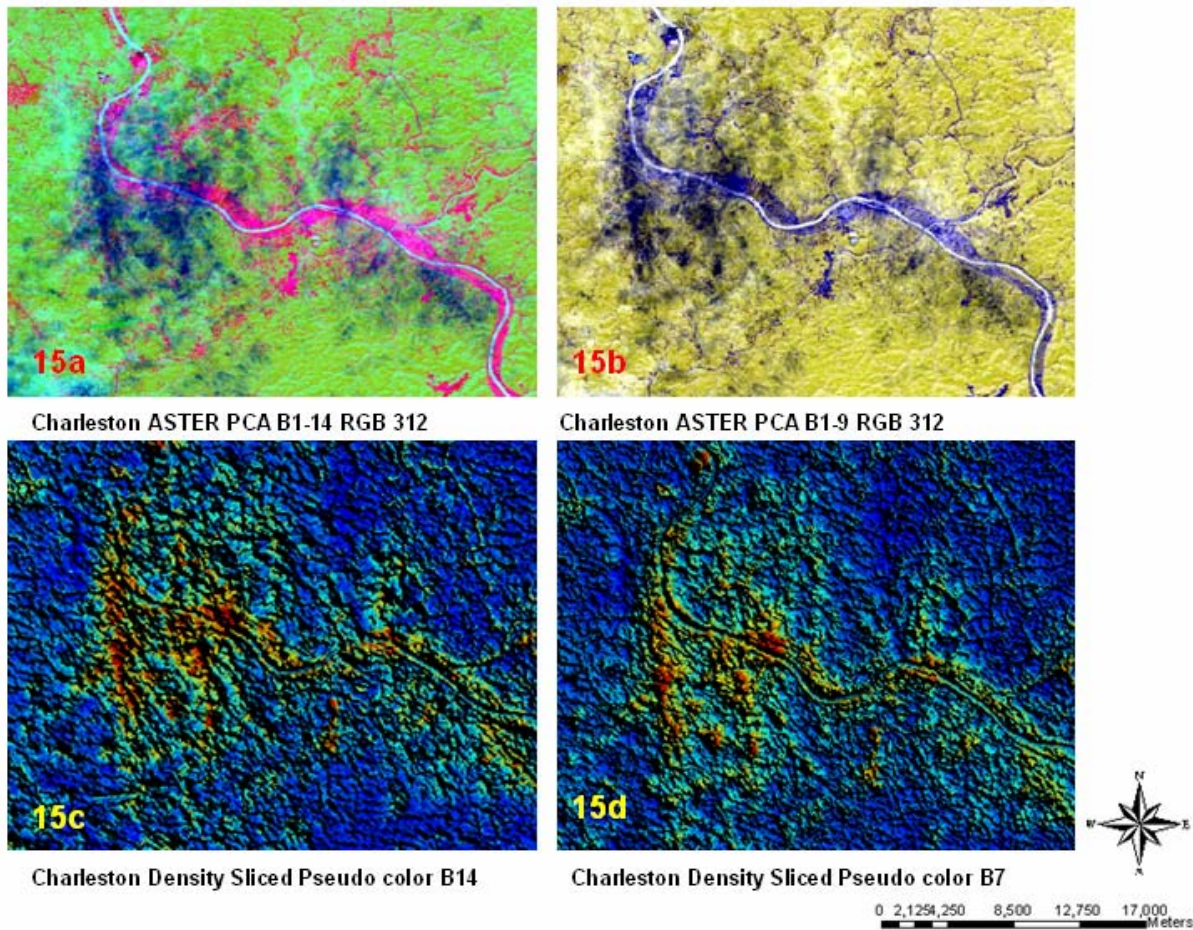
Figure 15: September 19, 2005, Charleston, WV area ASTER processed images: (a) PCA images in all 14 bands. (b) PCA image B-1-9 bands. (c): Density sliced band 14. (d): Density sliced band 7.

Spectral signatures of SWIR in bands 5, 7, and 8 shows little variations (Figure16a).

TIR bands 13 and 14 shows much absorption and variations (Figure16b).
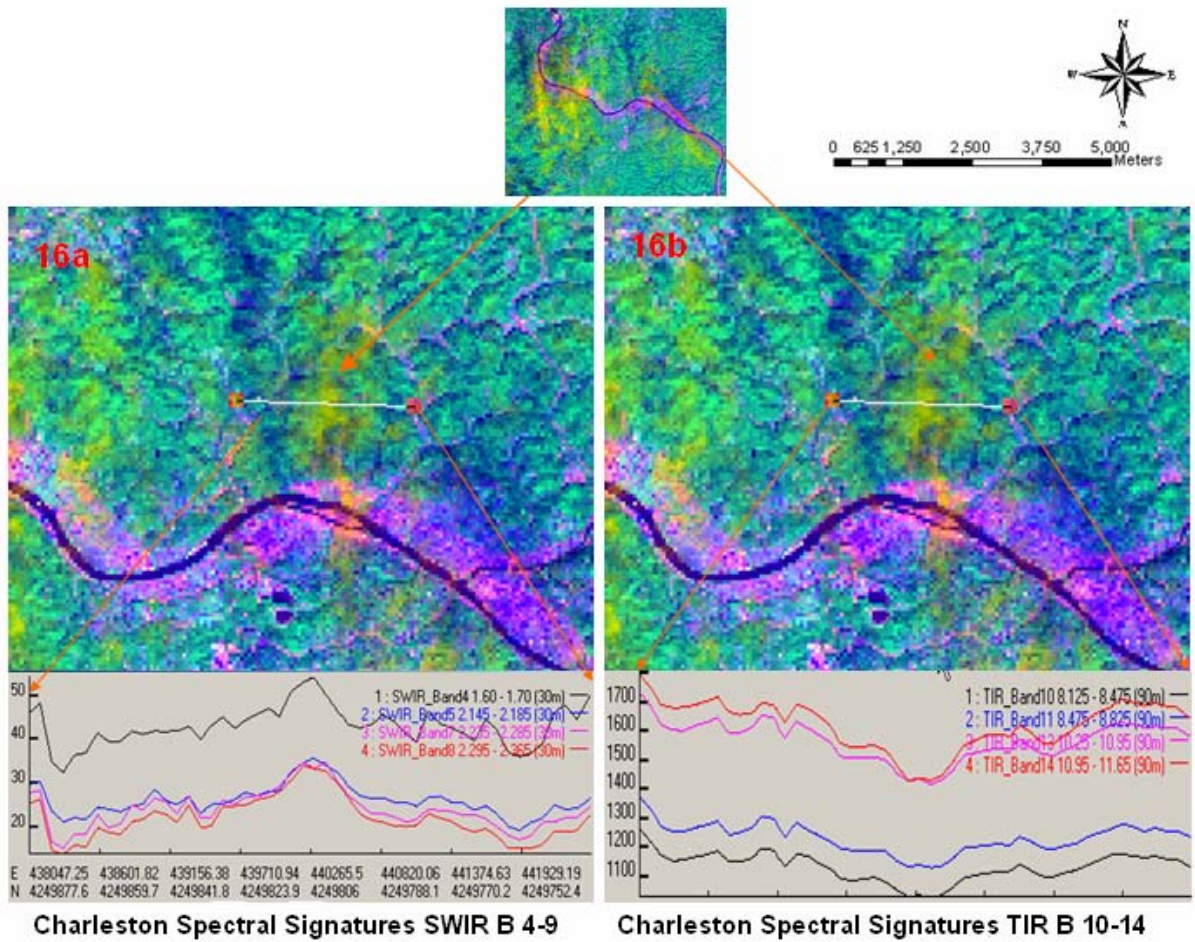
Figure 16: Spectral signatures of air pollutant over Gutherie Agricultural center in Charleston, WV area: (a) All SWIR B-4-9 are compared, shows variations in absorption. (b) All TIR bands B-10-14 are compared shows variations in absorption.

Band ratioing is applied with blue in TIR bands 14/10, green in SWIR bands 7/5 and red in VNIR bands 3/2 in the ASTER image of Charleston area, and the resultant image (Figure 17) shows different tones of yellow in the cloud mask over the city
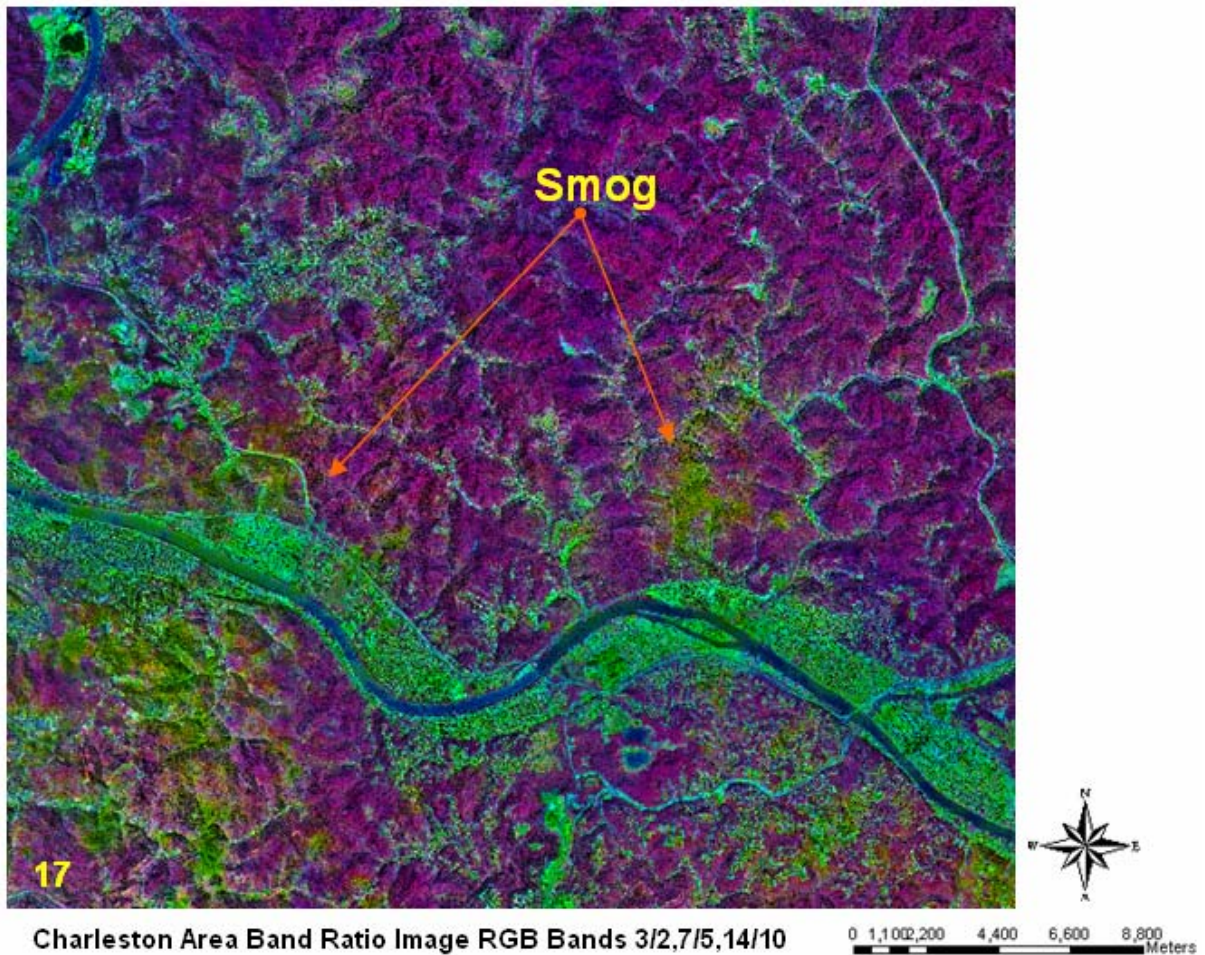
Figure 17: Band ratio image in RGB bands 3/2, 7/5, 14/10 of Charleston area highlighted plume over the city in different tone of yellow.

3.4. Statistical Analysis

3.4.1 Analysis of Variance:

Analysis of variance, or ANOVA, typically refers to partitioning the variation in a variable's values into variation among and within several groups or classes of observations. ANOVA is used to uncover the main interaction effects of categorical independent variables (called "factors") on an interval dependent variable.

ASTER pixel values in SWIR and TIR bands, of the EPA monitoring stations of each city are used as a dependant variable and EPA measurements of pollutants are as independent variables. Their statistical relations are established. There are different number of EPA monitoring station's air quality data, seven in Los Angeles, seven in San Francisco, and three in Charleston. Therefore there is unequal number of sample members per city; hence it is an unbalanced design. Therefore statistical procedure, 'Analysis of Variance' (ANOVA) by a 'general linear model' called 'PROC GLM' (general linear model) in SAS software (www.sas.com) is used in this investigation. The GLM procedure is generally used to perform simple or complicated ANOVA for balanced or unbalanced data (ANOVA Tutorial).

3.4.1.1. General Linear Model:

A linear model has been used in order to fit EPA in-situ data into ASTER pixel digital numbers data, (DNs) that include each 'City' as a blocking factor. The linear model relationship created is as follows:

(ASTER DNs) = A +B* (EPA Pollutant Concentration) + C * (City effect) + Residue

Where **A** = Intercept

B= Slope

C= Regional shift

All pixel values and pollutants concentrations levels are fed into PROC-GLM program in 'SAS' software and to establish a linear relationship. The interactions (Pollutant * City) were tested, with all SWIR and TIR bands (VNIR exception due to lower absorption

coefficient), with observed significance levels (p-value) in order to determine if the data meets an acceptance level of error (p-value equal to 0.005 as 95% probability).

Table-2: *Probability error level of in ASTER reflectance value in correspond to the EPA pollutants monitoring of CO, NOx and PM_10 and respective cities effect (from 'ANOVA' ProcGLM, Program in SAS software. This table contains p-values; non-significant (showed as dash in the table, if p>0.05. non-significant value type of data has no statistically significant effect on overall mean.*

Source	ASTER Bands									
	Short-wave Infrared Bands					Thermal Infrared Bands				
	B-5	B-6	B-7	B-8	B-9	B-10	B-11	B-12	B-13	B-14
CO	-	-	0.0162	-	-	0.0004	0.0003	0.0005	0.0005	0.0003
City Effect	0.0039	0.0036	0.0007	0.0094	0.0131	-	0.0177	0.0019	0.0013	0.0001
NOx	0.009	0.0044	0.0007	0.0041	0.0032	0.0001	0.0001	0.0001	0.0001	0.0001
City Effect	-	-	-	-	-	0.0015	0.0024	0.0007	0.0002	0.0001
PM_10	-	-	-	-	-	0.0164	0.0193	0.0466	0.0332	0.0236
City Effect	0.0133	0.0057	0.0098	0.0293	0.0233	0.0296	0.0147	0.0071	0.0044	0.001

The lower the p-values, the more likely the effect is significant. Values were removed from these models where they were not significant. All of the assumptions were tested for all models, and only channel 9 data had to be log-transformed in order to meet the assumptions of the ANOVA.

The statistical term 'Coefficient of Determination (R-Square) is a statistical term, which signifies total percentage of variations explained by the independent variable in the regression line, and rest of the variations is explained by another factor (not a linear relationship). Results from PROC GLM program in SAS software obtained were shown in

the Table-2. It is observed that there is significant city effect, which the results are not consistent among the cities (all channels for PM_10, all except Ch10 for CO, channels 10-14 for NOx). If the city effect is non-significant, the spectral response to the pollutant is consistent no matter where samples were found, and the data is collected (Ch10 for CO and channels 10-14 for NOx). In SWIR bands ASTER Channels 5 – 9 (Table2) shows no correlation with PM_10 concentrations, channel 7 was found weakly correlated with CO concentrations.

Table-3: *Coefficient of Determination (R-Square) values and Coefficient of Variance values from 'ANOVA' results of ASTER SWIR bands 5 through 9 reflectance values, and TIR bands 10 through 14, reflectance value in corresponds to the EPA pollutants monitoring of CO, NOx and PM_10 in respective cities (as block) (from 'ANOVA' ProcGLM, Program in SAS software).*

| Air Pollutants		ASTER Bands									
		Short-wave Infrared Bands					Thermal Infrared Bands				
		B-5	B-6	B-7	B-8	B-9	B-10	B-11	B-12	B-13	B-14
CO	R-Square	0.57803	0.57972	0.69101	0.52166	0.48791	0.68999	0.72365	0.75932	0.76195	0.81558
	Coeff. Variance	12.3828	14.7385	12.3154	16.769	15.9575	8.12486	8.54938	8.77929	7.65099	8.10207
NOx	R-Square	0.56603	0.62248	0.67411	0.17875	0.56584	0.75379	0.77286	0.81721	0.86425	0.88177
	Coeff. Variance	12.5575	13.9687	12.6479	17.1165	5.48549	7.24071	7.75075	7.65095	5.77764	6.48716
PM_10	R-Square	0.50157	0.54904	0.51235	0.42463	0.44043	0.46732	0.50151	0.29548	0.5695	0.65291
	Coeff. Variance	13.4579	15.2669	16.769	18.3913	6.22757	10.6503	11.4823	55.5199	10.289	11.1151

All 5 SWIR channels indicate correlations with NOx levels. In TIR bands, ASTER channel 10-14, the relationship between spectral values and CO or NO_X were highly significant.

PROC-GLM runs in all channels with blocking and interaction terms, and shows the Coefficient of Determination (R-Square's) (Table 3) in SWIR channel 7 and 14 has higher values. In channel 7, R-Square found for CO, NOx, and PM_10 were nearly the same. In Channel 14, R-Square is found in PM_10 is nearly significant, while that of CO and NOx are more highly significant, showing sensitivity of band 14 for CO and NOx.

Both ANOVA results and scatter plot of pollutants with ASTER DNs shows no correlation in SWIR 5-9 bands with EPA monitored PM_10 concentrations and it is also evident from the fact that there is no absorption band for PM_10 in any of the ASTER bands. Very weak absorption band of CO at 2.31 μ m and weak correlation in ANOVA result in channel 7 with EPA CO concentrations was expected. With correlations observed by all 5 SWIR channels with NOx levels and spectral signature of the nine components of NOx, it is difficult to say about which component of NO_X, as they are most unstable, is active in the atmosphere (Winnewisser et al., 2004). In TIR bands, ASTER channel 10-14, NO_X and CO were found highly significant, although there is a strong absorption band for HNO3 at 11 μ m in ASTER band 14, but there is no absorption band for CO in ASTER TIR bands. Therefore in view of ANOVA results, there could be something similar to CO in the sample. Weak correlation of PM_10 in ANOVA result with TIR channels but high absorption bands of PM_10 in the 10-13 μ m band, contradicts smog detection with other techniques mentioned in the manuscript. It may be due to the fact that there were fewer number of EPA monitoring stations and monitoring is far away from the source. The possible wind factor that causes transport of pollutant over longer distances may provide for photochemical mix and dilution of samples.

3.4.2 Scatter Plot of Variance:

Scatter plots of Pollutant concentration with ASTER pixel digital data numbers are

18(a1)

18(a2)

18(b1)

18(b2)

18(c1)

18(c2)
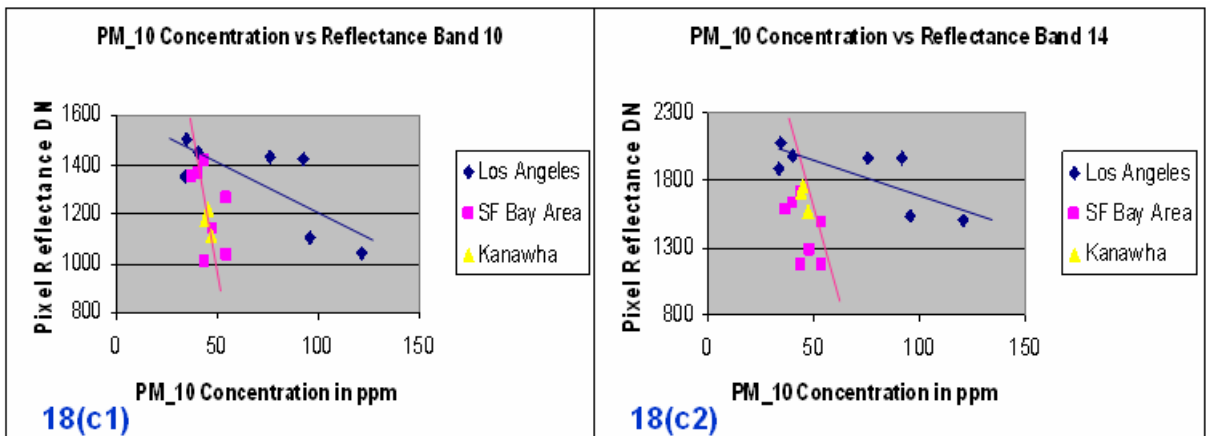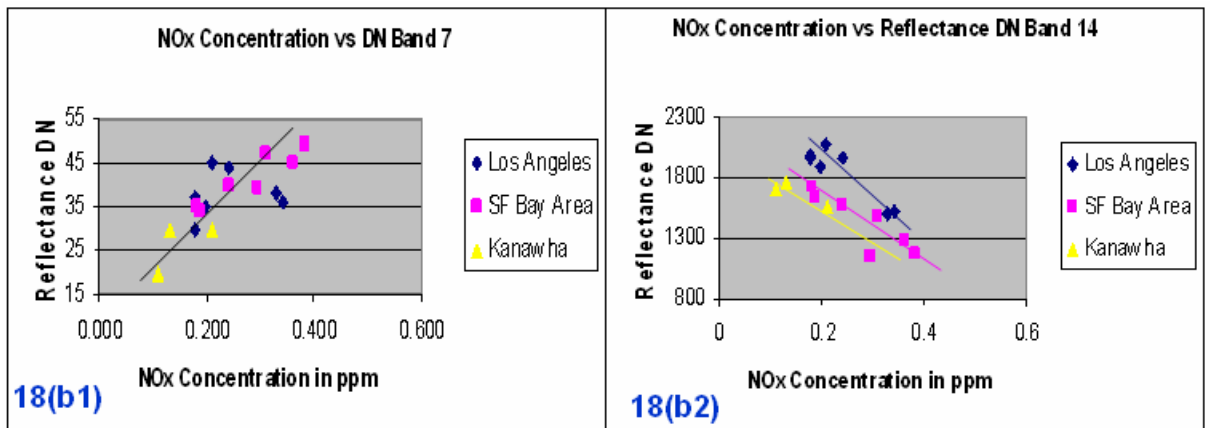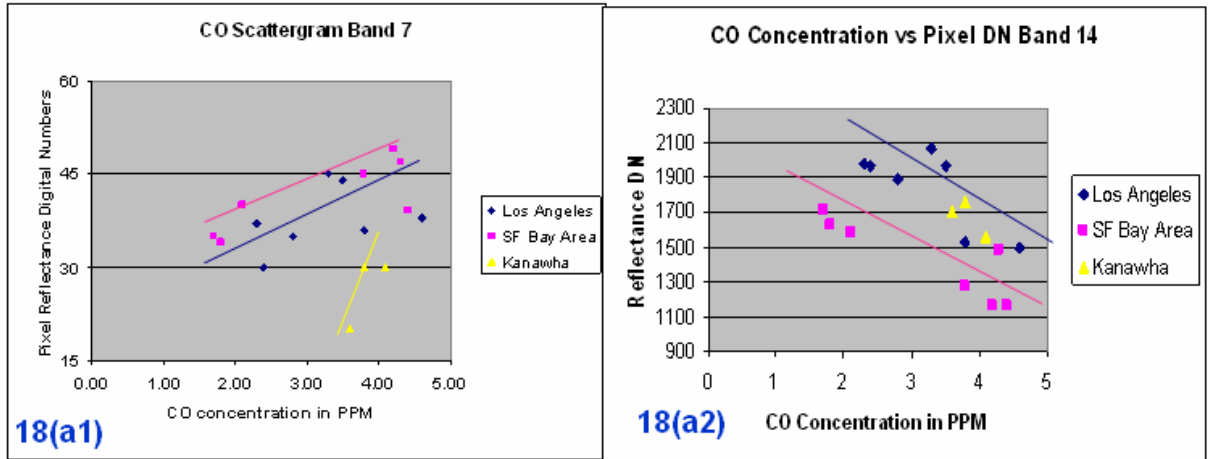
Figure 18: Scatter plot of EPA pollutant Concentration level at San Francisco Bay area, Los Angeles area, and at Charleston area against respective sites ASTER digital numbers in bands 14 and 7: (a1) and (a2) CO in band 7 and 14 respectively. (b1) and (b2) NOx in bands 7 and 14 respectively. (c1) and (c2) PM_10 in bands 7 and 14 respectively.

created for, CO, NOx and PM_10 of in bands 7 and 14, where high correlations were observed. Results shown in the scatter plots (Figure18) suggest city wise regional shifts in correlation of data swarm. For CO in band 7, Los Angeles and San Francisco Bay area are weakly correlated (Figure 18a1). Band 14 shows a high correlation in San Francisco area, but a very weak negative correlation for Los Angeles and Charleston (Figure 18 a2). For NOx in band 7 San Francisco and Charleston are highly correlated (Figure18 b1), but in Los Angeles very weak correlation is observed. NOx in band 14, Los Angeles and San Francisco are negatively correlated with different correlation lines. In Charleston for band 14, no prediction can be made due to fewer numbers (only 3) of monitoring station data. PM_10 for band 10, San Francisco, Los Angeles and Charleston are not correlated in a linear model (Fig.18c1). PM_10 for band 14 there is a weak negative correlation observed in Los Angeles, but very low correlation in both Charleston and San Francisco.

3.5 High-frequency Filtering

Analysis of variance suggests that TIR band 14 is highly correlated with EPA concentration in NOx and PM_10. Also SWIR band 7 is correlated with EPA CO concentration level.

19(a1)

Bay Area RGB 3,7,14 Without Filter

High Pass
Filter

19(a2)

Bay Area RGB 3,7,14 With Filter

0 7,500 15,000   30,000   45,000   60,000
Meters

19(b1)

Los Angeles RGB 3,7,14 Without Filter

High Pass
Filter

19(b2)

Los Angeles RGB 3,7,14 With Filter

0 2,700 5,400   10,800   16,200   21,600
Meters

19(c1)

Charleston RGB 3,7,14 Without Filter

High Pass
Filter

19(c2)

Charleston RGB 3,7,14 With Filter
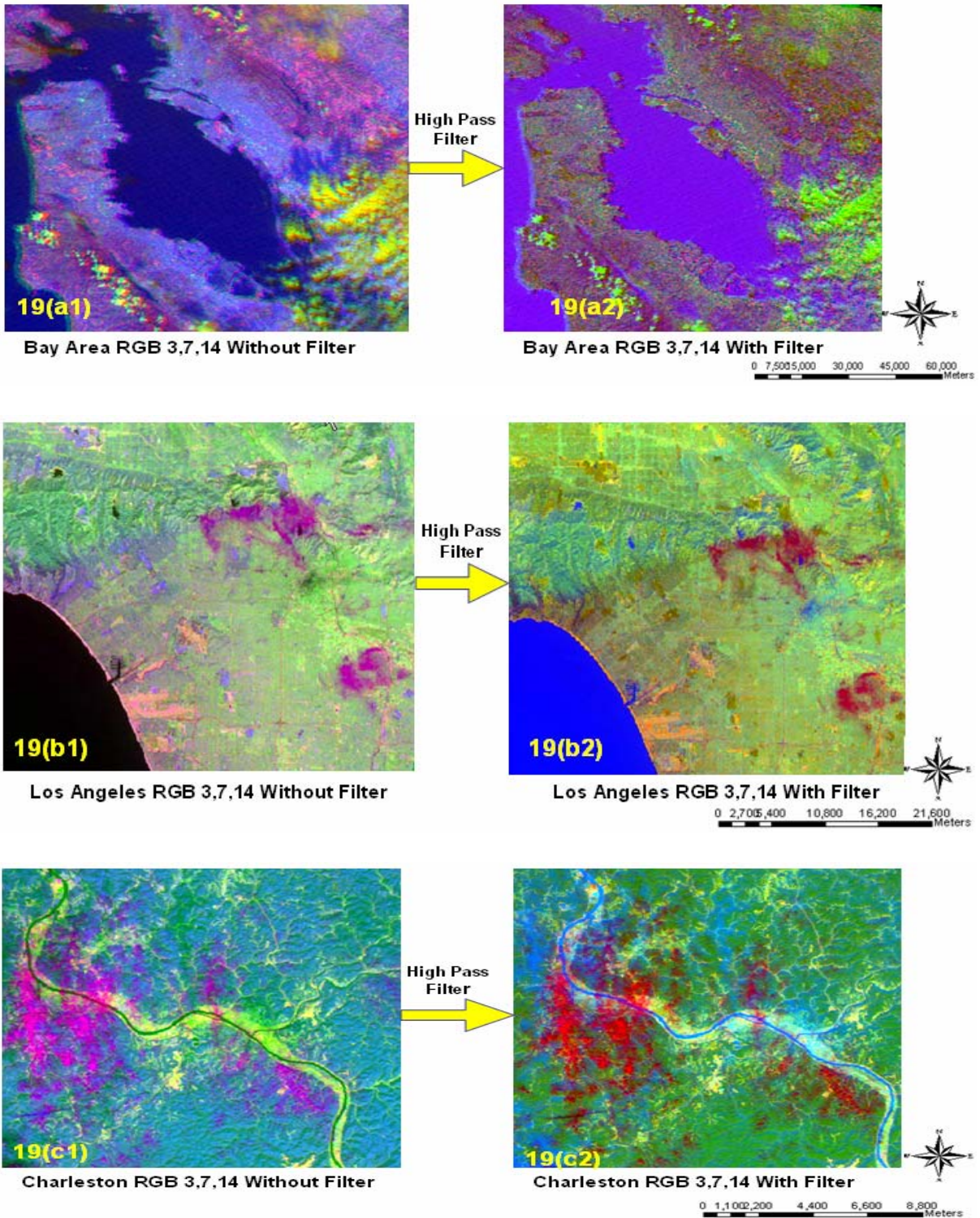
0 1,100 2,200   4,400   6,600   8,800
Meters

Figure 19: High band-pass filter, with ASTER digital numbers in band 14, 7, and 3, applied on ASTER images: (a1) San Francisco Bay area in RGB 3,7and14 without filter. (a2) San Francisco in RGB 3,7, 14 after filter is applied. (b1) Los Angeles area in RGB 3,7, 14

41

without filter. (b2) Los Angeles area in RGB 3,7, 14 after filter is applied. (c1) Charleston area in RGB 3,7, 14 without filter. (c2) Charleston area in RGB 3,7, 14 after filter is applied.

Therefore a spatial filtering technique is applied with those bands pixel digital numbers to enhance high frequency local variations. A very rough convolution mask of 3x3 kernel size has been used with a center value as the digital number of the pixel in TIR band 14, SWIR band7, and VNIR band 3 in all the image data set. The resultant images are shown in Figures 19 (a1 through c2). The entire filtered images interface between regular cloud pattern and plumes are almost distinguishable. Also in Bay area filtered image (Figure19 (a2)) coastal water pollutants are slightly distinguishable.

In the Los Angeles image before filtering (Figure 19-b1) does not show pollution patterns over West Los Angeles. It shows only in Lynwood area and Los Angeles downtown area. The filtered image (Figure 19-b2) shows a plume pattern in West Los Angeles. In Charleston different tones of cloud pattern (Fig. 19-c2) in the atmosphere are highlighted in the filtered image suggesting cloud pollution mixing due to prevailing wind patterns through the valley.

Chapter 4

Summary and Conclusion

This research investigation presents a methodology to assess atmospheric pollution from a multi-spectral satellite platform. Several image processing techniques were used to extract features for pattern recognition. In the research investigation resolves differences in pollution absorption patterns with the relatively wide wavelength bands of ASTER. PCA, density slicing. Band ratioing, spectral signatures in different bands, and High-pass band filtering images, demonstrated many different kinds of pollutant patterns in different cities under investigation. The GIS map of San Francisco Bay area with EPA monitoring sites suggests that there are multiple sources of air pollutants there. Variable wind speed and direction in a high land-locked area of San Francisco Bay may cause the transport of air pollutants from their source to longer distances. The PCA image of San Francisco with all ASTER bands using density sliced image in band 14, absorption differences of pollutants in TIR band 14 is observed. The absorption difference was found to be weak in ASTER band 7. Also variations detected in spectral signatures were stronger in TIR and weaker in SWIR. Separation of regular cloud patterns and pollution sources plumes of CCN in the band ratio images and other evidence given above, suggest that there may be PM_10 and some carbonates in the cloud pattern over San Francisco Bay area on March 10, 2000.

The GIS map of Los Angeles area and EPA monitoring data suggest that there are multiple sources of air pollutants there. Variable wind speed and direction in Los Angeles may cause the transport of air pollutants from their source to longer distances eastward. The PCA image, Density sliced images, spectral signatures in SWIR and VNIR bands of Los

Angeles suggest that there is high concentration of PM_10 in the atmosphere over the Commerce, Lynwood and Los Angeles commercial district. More accurate and detailed information on air pollutants patterns can be assessed using hyperspectral data. Future research investigations will focus on hyperspectral studies in order to find the subtle differences in spectral signature of atmospheric constituents and pollutants.

The GIS map of the Charleston area with industry data from WVDEP and EPA monitoring data, indicate multiple sources of air pollutants. With wind patterns in a valley area as Kanawha Valley in Charleston West Virginia, suggests that air pollutant emission from various sources may remain confined to the valley and eventually go back to the earth surface with precipitation. The PCA image, Density sliced image, spectral signatures in SWIR and VNIR bands of Charleston area suggest that there is high concentration of PM_10 and carbonates in the atmosphere over Charleston area.

Statistical analysis support different feature extraction patterns of different kinds of air pollutants in the atmosphere of San Francisco, Los Angeles and Charleston. More accurate and detailed information on air pollutants patterns can be assessed using hyperspectral data. Future research will focus on hyperspectral research to investigate the subtle differences in spectral signature of atmospheric pollutant patterns using feature extraction and pattern recognition techniques in advanced satellite sensor image systems and nanotechnology based sensors.

References

1. ANOVA Tutorial: See http://www.ats.ucla.edu/STAT/sas/library/repeated_ut.htm

2. ASTER, NASA, 2000: ASTER user guide, NASA, 2000.

3. Belsma Leslie O., 'Satellite Data for Air Quality Forcaster', The Aerospace Report. 2004

4. Brumfield J. O. and Ralph Oberly: Illustrating Physical Principles through comparative feature extraction techniques in optical and digital image processing: Society of photo optical engineers at international conference on Optics in Education in Leningrad, se. 28- ct.01, 1991.

5. Chung C. E. and V. Ramanathan, South Asian Haze Forcing: Remote Impact with Implications to ENSO and AO, American Meteorological Society, June 2003, p-1791-1806

6. EPA: Criteria Pollutant report http://www.epa.gov/airtrends/aqtrnd98/chapter2.pdf, 1998.

7. EPA Air Resources Board: State and Local Monitoring Network Report manual, October 2005.

8. ER-Mapper Inc., 2006. See www.ermapper.com

9. HITRAN: High-resolution Transmission Molecular Absorption database, see www.hitran.com

10. Jensen, J. R.: Introductory Digital Image Processing: A Remote Sensing Perspective, Prentice Hall, 2005.

11. Jacob, D.J., B.D. Li, Q. Blake, D. R. de Gouw, J. Warneke, C. Hansel, A. Wisthaler, A. Singh, H.B. Guenther: Global budget of methanol: Constraint from atmospheric observations, J. Geophys. Res., 110, D08303, doi: 10.1029/2004JD005172, 2005.

12. USGS-Landsat, 1998: See the website: http://landsat7.usgs.gov/

13. Lee Y.S., D. R. Collins, Feingold, G. "Derived Optical and cloud nucleating properties of biomass burning aerosol from the May, 2003 fires in the Yucatan," 23rd Annual American Association for Aerosol Research Meeting, October, 2004.

14. Maziere M. De et al. : Regional monitoring of troposphere NO2 and CO2 using Remote Sensing from high altitude platforms- Preliminary concept, Belgian Institute for space Aeronomy, Brussles, 2005.

15. Menon Surabi, James Hansen, Larissa Nazarenko, and Yunfeng Luo: Climate effects of Black Carbon Aerosols in China and India, Sciencemag.org, Vol-297, September 27, 2002.

16. NASA Tutorial: See the web NASA site give below: http://idlastro.gsfc.nasa.gov/idl_html_help/Filtering_an_Imageiry.html

17. OSU-Climate Group: The Ohio State University Climate Group: See: http://www-bprc.mps.ohio-state.edu/Icecore/Abstracts/Publications.html

18. Pacific Steel Casting Company, Berkeley, CA 94710, Summary of Pacific Steel Casting's proposed odor control plan, http://www.pacificsteel.com/OdorControlPlan-Summary&Plan%202005.pdf. 2005.

19. Perrin, A., J. Orphal, J.M. Flaud, S. Klee, G. Mellau, H. Mader, D. Walbrodt, and M. Winnewisser. : New Analysis of the v5 and 2V9 bands of HNO3 by infrared and

millimeter wave techniques: Line position and intensities, Journal of Molecular Spectroscopy 228 (2004), p-375-391, 2004.

20. Petaja T., Kerminen V.M, Hameri K, Vaattovaara P: Effects of SO2 Oxidation on ambient aerosol growth in water and ethanol vapors: Atmospheric Chemistry and Physics-5, p- 767-779, 2005

21. Pope, C. A., III, Review: Epidemiological basis for particulate air pollution health standards, Aerosol. Sci. Technol., 32(1), 4-14, 2000.

22. Ramanathan, V. Satheesh, S.K. Large Differences in Tropical Aerosol Forcing at the Top of the Atmosphere and Earth's Surface, Nature, 405, 60, 2001.

23. Ramanathan, V. and M.V. Ramanna: Atmospheric Brown Clouds: Long-Range Transport and Climate Impacts, EM December 2003.

24. RETALIS, A: Assessment of the distribution of aerosols in the area of Athens with the use of Landsat Thematic Mapper data: International Journal of Remote Sensing, p-939 – 945. Taylor & Francis Volume 20, Number 5 / March 20, 1999.

25. Roy, P., J.O. Brumfield, R. Oberly, and A. Vaseashta: Smog Extraction in Urban Area using ASTER and its Correlation with In-situ Data, International Nanotechnology Congress, Nov. 2nd, 2006, International Association of Nanotechnology: See www.ianano.org

26. Sifakis N. I., N.A. Soulakellis, in 'Satellite Image Processing for Haze and Aerosol Mapping (SIPHA): Code Description and presentation of results, Institute of Space Application & Remote Sensing, National Observatory of Athens: European Commission funded research, Contract number 94/.GR/A32/GR/01616/ATT. See http://www.space.noa.gr

27. Schafer , K. G. Fömmel[1], H. Hoffmann, S. Briz, W. Junkermann, S. Emeis, C. Jahn, S. Leipold, A. Sedlmaier, S. Dinev, G. Reishofer, L. Windholz, N. Soulakellis, N. Sifakis and D. Sarigiannis. : Three-Dimensional Ground-Based Measurements of Urban Air Quality to Evaluate Satellite Derived Interpretations for Urban Air Pollution: Springer, Vol. 2, Number 5-6, September 2002.

28. UNEP: Atmospheric Brown Clouds, 2005 under the sponsorship of the United Nations Environmental Program and NOAA. See http://www.sianbrowncloud.ucsd.edu/.

29. UNEP Assessment Report, 2004: See the website: http://www.rrcap.unep.org/abc/impactstudy/Part%20I.pdf.

30. Ung Anthony, Lucien Wald, Thierry Ranchin, Joseph Kleinpeter: Air pollution mapping: Relationship between satellite-made observations and air quality parameters, 12th International Symposium, Transport and Air Pollution, 16-18 June 2003, p-105-111.

31. Vaseashta, A. and J. Irudayaraj : Nanostructured and Nanoscale Devices and Sensors, Journal of Optoelectronics & Advanced Materials Vol. 7, No. 1, p. 35-42, 2005.

32. Vaseashta et al. Nanostructured and Advanced Materials for Applications in Sensor, Optoelectronic and Photovoltaic Technology, Springer (2005).

33. Vaseashta, A., J.O. Brumfield, S.B. Vaseashta, J. Barrios, and P. Roy: Atmospheric Parameters Sensing Using Nanotechnology Based Sensors and Image Processed Real-Time Satellite Data, at Kassing et al. (eds.), Functional Properties of Nanostructured Materials, p- 443-448, Springer, Netherlands, 2006.

34. WHO, 2000, Guidelines for Air Quality, World Health Organization Report, Geneva, 2000.

35. Winnewisser M. Perrin A. Orphal J.: New Analysis of the V5 and 2V9 bands of HNO3 by infrared and millimeter wave techniques: Line position and intensities; Luornal of Molecular Spectroscopy 228; p375-391, 2004.

36. Xu, L. H., Lees R.M, Wang P., Brown L.R., Kleiner I. And Johns J. W. C.: New assignments, line intensities, and HITRAN database for methanol at 10μm, J. Mol. Spectroscopy., 228,453-470, 2004.

37. Yu H. Y.J. Kaufman, M. Chin, G. Feingold, M. Zhou: A Review of Measurement-based Assessment of Aerosol Direct Radiative Effect and Forcing, Atmospheric Chemistry and Physics, May 2005.